MAIT cells monitor intestinal dysbiosis and contribute to host protection during colitis

Yara El Morr, Mariela Furstenheim, Martin Mestdagh, Katarzyna Franciszkiewicz, Marion Salou, Claire Morvan, Thierry Dupré, Alexey Vorobev, Bakhos Jneid, Virginie Premel, et al.

MAIT cells monitor intestinal dysbiosis and contribute to host protection during colitis

Authors Yara El Morr[#1], Mariela Fürstenheim[#1,2], Martin Mestdagh[1], Katarzyna Franciszkiewicz[1], Marion Salou[1], Claire Morvan[3], Thierry Dupré[4], Alexey Vorobev[1], Bakhos Jneid[1], Virginie Premel[1], Aurélie Darbois[1], Laetitia Perrin[1], Stanislas Mondot[5], Ludovic Colombeau[6], Hélène Bugaut[1], Anastasia du Halgouet[1], Sophie Richon[7], Emanuele Procopio[1], Mathieu Maurin[1], Catherine Philippe[5], Raphael Rodriguez[6], Olivier Lantz[1,8,9*] and François Legoux[1,10*, &].

Affiliations
[1]Institut Curie, PSL University, Inserm U932, Immunity and Cancer, Paris, France
[2]Université Paris Cité, Paris, France
[3]Institut Pasteur, Université Paris Cité, UMR CNRS 6047, Laboratoire Pathogenèse des Bactéries Anaérobies, F-75015 Paris, France.
[4]Laboratoire de Biochimie, Hôpital Bichat AP-HP, Université de Paris, Paris, France.
[5]Institut Micalis, INRAE, AgroParisTech, Université Paris-Saclay, Jouy-en-Josas, France
[6]CNRS UMR 3666, INSERM U1143, Chemical Biology of Cancer Laboratory, PSL University, Institut Curie, 75005 Paris, France.
[7]Institut Curie, PSL Research University, CNRS UMR144, Paris, France
[8]Laboratoire d'immunologie clinique, Institut Curie, Paris, 75005, France.
[9]Centre d'investigation Clinique en Biothérapie Gustave-Roussy Institut Curie (CIC-BT1428)
[10]INSERM ERL1305, CNRS UMR6290, Université de Rennes, Institut de Génétique & Développement de Rennes, France

[#] Equal contribution
[*] Corresponding authors
[&] Lead contact: Francois.Legoux@inserm.fr

Summary
Intestinal inflammation shifts microbiota composition and metabolism. How the host monitors and responds to such changes remains unclear. Here, we describe a protective mechanism by which Mucosal-associated invariant T (MAIT) cells detect microbiota metabolites produced upon intestinal inflammation and promote tissue repair in return. At steady-state, MAIT ligands derived from the riboflavin biosynthesis pathway were produced by aerotolerant bacteria residing in the colon mucosa. Experimental colitis triggered a luminal expansion of riboflavin-producing bacteria, leading to increased production of MAIT ligands. Modulation of intestinal oxygen levels suggested a role for oxygen in inducing MAIT ligand production. MAIT ligands produced in the colon rapidly crossed the intestinal barrier and activated MAIT cells, which expressed tissue-repair genes and produced barrier-promoting mediators during colitis. Mice lacking MAIT cells were more susceptible to colitis and colitis-driven colorectal cancer. Thus, MAIT cells monitor a bacterial metabolic pathway indicative of intestinal inflammation.

One-sentence summary

Beneficial MAIT cell - microbiota interactions during intestinal inflammation

Keywords

Microbiota, colitis, dysbiosis, MAIT, meta-transcriptomics, colon cancer

Introduction

Many human diseases are associated with changes in the composition and activity of the intestinal microbiota. At steady-state, the host controls critical nutrients availability to allow the growth of beneficial microbes and to contain the expansion of potentially harmful bacteria. The abundance of electron acceptors, such as oxygen and nitrates in the colon lumen, has emerged as a key ecological parameter that shapes microbiota composition(*1*). At steady-state, oxygen coming from the blood is consumed by the colon epithelium, effectively maintaining a hypoxic luminal environment that selects for fermentative, strict anaerobic bacteria such as *Firmicutes* and *Bacteroidetes*(*2*). By contrast, the availability of oxygen in the lumen (dysanaerobiosis) enables bacterial respiration, a metabolism that yields more energy than fermentation and fuels the expansion of facultative anaerobes such as *Enterobacteriaceae*(*1*). Dysanaerobiosis represents a major driver of dysbiosis and underlies many pathological situations such as inflammatory bowel diseases (IBD), enteric infections and colorectal cancer (CRC)(*3*). Whether the host monitors microbial metabolites indicative of intestinal dysbiosis remains unclear.

MAIT cells are innate-like T cells that recognize microbial metabolites presented by the MHC-related molecule MR1 and that are abundant in liver and mucosal tissues (10-40% of T cells in liver, 1-10% in gut). The particular tissue location of MAIT cells suggests a key role in the surveillance of microbiota-derived ligands produced by the intestinal microbiota(*4*). MAIT ligands derive from the riboflavin precursor 5-Amino-6-(D-ribitylamino)uracil (5-A-RU), which reacts with methylglyoxal or glyoxal to generate the potent antigens 5-(2-oxopropylideneamino)-6-D-ribitylaminouracil (5-OP-RU) and 5-(2-oxoethylideneamino)-6-D-ribitylaminouracil (5-OE-RU). 5-A-RU is synthesized by the microbial enzyme RibD, which is strictly necessary for the production of MAIT ligands in both Gram+ and Gram- bacteria(*5*, *6*). The amount of bacterial MAIT ligands produced is proportional to the amount of riboflavin produced(*7*), suggesting that MAIT cells may become activated through the T cell receptor (TCR) in the context of strong microbial riboflavin production. However, the rules governing riboflavin production by the microbiota are unknown. Riboflavin is the precursor of flavin mononucleotide (FMN) and flavin adenine dinucleotide (FAD), two major coenzymes involved in many redox reactions owing to their ability to shuttle electrons from donor to acceptor molecules. FAD is an essential component of the complex II in the respiratory electron transport chain(*8*). Thus, intestinal dysanaerobiosis may increase riboflavin needs and lead to MAIT ligand synthesis by the microbiota.

In support of this hypothesis, MAIT cells are activated in pathologies associated with intestinal dysanaerobiosis, such as IBD(*9*, *10*) and CRC(*11–13*), in which the intestinal microbiota is enriched in bacteria capable of riboflavin synthesis(*14–16*). TCR stimulation of MAIT cells drives expression of tissue-repair genes(*17, 18*) and can accelerate the growth of an intestinal epithelial cell line(*17*). Yet, the exact role of MAIT cells in IBD is unknown.

In this study, we used a meta-transcriptomic approach coupled with a highly specific MAIT ligand quantification assay to investigate the effect of intestinal inflammation on the production of riboflavin and MAIT ligands in the gut. We found that MAIT ligands were synthesized by aerotolerant bacteria that bloom in the gut lumen during experimental colitis. The subsequent MAIT cell activation lead to the production of anti-inflammatory and tissue-repair mediators. Mice

lacking MAIT cells were more susceptible to chronic colitis and colitis-induced colorectal cancer strongly suggesting that MAIT cells reduce intestinal inflammation.

Results

Bacterial production of MAIT ligands in the colonic mucosa

To quantify MAIT ligands in the large intestine, we adapted a sensitive *in vitro* bioassay(*6*) based on the activation of mono-specific TCR transgenic (Tg) T cells recognizing the canonical MAIT ligand 5-(2-oxopropylideneamino)-6-D-ribitylaminouracil (5-OP-RU)(*19*). The mouse embryonic fibroblast cell line WT3, engineered to over-express MR1(*20*), was used as MAIT antigen-presenting cells. WT3-MR1 cells loaded with synthetic 5-OP-RU efficiently induced CD25 and CD69 at the surface of tetramer$^+$ 5-OP-RU-specific TCR-Tg T cells after overnight co-culture (Fig. S1A-B). To assess the presence of MAIT ligands in the intestine, colon contents from a B6 mouse were solubilised in culture medium, passed through a 0.22 μm filter to eliminate bacteria and incubated with wild-type WT3 cells (which express low levels of MR1) or WT3-MR1 cells. The antigen-loaded cells were then washed and incubated overnight with TCR-Tg T cells (Fig. 1A). 5-OP-RU-specific TCR-Tg T cells expressed CD25 and CD69 after co-culture with WT3-MR1, but not WT3 cells, indicating cognate activation by MR1-restricted MAIT ligands (Fig. 1A). Using a standard curve of synthetic 5-OP-RU, the concentration of MAIT ligands was estimated at 0.8 pmol/g of cecum contents, 1.8 pmol/g of colon contents and 7 pmol/g of feces (Fig. 1B). Both fungi and bacteria can produce riboflavin-derived MAIT ligands(*5*). MAIT ligands were depleted from intestinal contents when mice were treated with broad-spectrum antibiotics (Fig. 1B), but not with the anti-fungal drug fluconazole (Fig. S1C), indicating that MAIT ligands were mostly produced by the commensal bacteria.

The large intestine presents ecological niches populated by microbial communities with distinct metabolic requirements(*21*), which could affect MAIT ligand production. In particular, oxygen arriving from the blood partially diffuses through the colon epithelium into the lumen, creating a steep oxygen gradient from the mucosal surface to the lumen that shapes microbial communities(*22*). We evaluated how the radial partitioning of the gut microbiota affects MAIT ligand production. While mucosal scrapes contained fewer bacteria (Fig. 1C), they were nonetheless more potent than lumen samples at activating 5-OP-RU-specific TCR-Tg T cells (Fig. 1D), indicating stronger MAIT ligand production in the mucosal side compared to the lumen. To explore mechanisms underlying increased MAIT ligand production in the mucosa, we sequenced the 16S rRNA genes and used PICRUSt(*23*) to estimate the metabolic potential of lumen and mucosa-associated bacterial communities. Mucosal communities were enriched in *Proteobacteria* (Families *Oxalobacteraceae* and *Enterobacteriaceae*) and *Deferribacteres* (Family *Deferribacteraceae*) (Fig. 1E, S1D and Table S1). In agreement with higher MAIT ligand production in the mucosa, PICRUSt predicted an enrichment in the riboflavin biosynthetic pathway in the mucosa as compared to the lumen (Fig. S1E). The oxidative phosphorylation and glutathione metabolisms were also enriched in mucosa (Fig. S1E), consistent with higher oxygen levels in the mucosa than in the lumen.

To directly quantify the transcriptional activity of the riboflavin biosynthetic pathway, we next sequenced the non-ribosomal RNAs from both the mucosa and the lumen. Metatranscriptomic analyses identified a number of bacterial genes (Fig. S2) and pathways (Fig. 1F) modulated

between the two locations and revealed higher expression of the riboflavin biosynthesis pathway in the mucosa as compared to the lumen (Fig. 1F). In particular the gene *ribD*, which controls production of the MAIT ligand precursor 5-A-RU, was over-expressed in the mucosa (Fig. 1G), consistent with active synthesis of MAIT ligands. Thus, the activity of the riboflavin biosynthesis pathway and the concentration of MAIT ligands vary in the distinct ecological niches of the gut and are higher in mucosal layers than in the lumen.

To identify the bacterial taxa contributing to MAIT ligand biosynthesis in the gut, we analyzed the taxonomy of *ribD* transcripts. In the lumen, *ribD* was mostly expressed by *Proteobacteria* and *Firmicutes* (Fig 1H and S1F). At the family level, the *Proteobacteria* were identified as *Desulfovibrionaceae*, while the *Firmicutes* could not be identified (Fig. S1F). In the mucosa, *ribD* reads were primarily expressed by *Deferribacteres* (Family *Deferribacteraceae*) and *Proteobacteria* (Family *Desulfovibrionaceae*). Intriguingly, both taxa represented minor components of the total metatranscriptome (Fig. 1H), suggesting that MAIT ligand production may be dominated by few strong producers. At the species level, *ribD* reads from the mucosa were mapped to *Mucispirillum schaedleri* (Fig. 1I), the only member of the *Deferribacteres* living in the mammalian intestine. *M. schaedleri* is found in most mammals (including humans) and resides in crypts and mucus layers(*24*) owing to its ability to scavenge oxygen and resist oxidative stress(*25*). In the mucosa, *M. schaedleri* indeed expressed a catalase, which protects against oxidative damage by reactive oxygen species, and the high-affinity cbb3-type cytochrome *c* oxidase, which can be used either for protection from O_2 stress or for micro-aerobic respiration(*25*) (Fig. S1G). Thus, the strong riboflavin biosynthesis pathway activity in the mucosa may reflect strong needs for riboflavin in microbiota living in an oxygen-exposed environment.

Dysanaerobiosis drives microbiota production of MAIT ligands

In neonates, intestinal hypoxia is not yet established and the colon presents higher abundance of facultative anaerobes such *as Enterobacteriaceae*, as compared to adults(*26*). MAIT ligands were more abundant in the colon of 2 weeks-old neonates as compared to 3 months-old adults, consistent with a link between intestinal oxygen levels and MAIT ligand production *in vivo* (Fig. S3A). In adults, intestinal hypoxia is maintained by epithelial cells through the β-oxidation of the butyrate(*2*, *27*). Colon oxygen levels can be modulated through the streptomycin-mediated depletion of butyrate-producing bacteria(*27*, *28*). To increase oxygen levels in the gut, adult mice were treated with streptomycin, resulting in reduced butyrate concentrations in the cecum (Fig. 2A). To quantify hypoxia in the colon, we used the exogenous oxygen-sensitive dye pimonidazole, which is retained in tissues at oxygen concentrations <1%(*28*). Pimonidazole was retained at the surface of colonocytes in non-treated mice (Fig. S3B), confirming epithelial hypoxia. Streptomycin treatment reduced pimonidazole staining (Fig. 2B), indicating increased colon oxygenation in these mice. Loss of hypoxia led to increased production of MAIT ligands, which concentrations increased 10-fold in the cecum (Fig. 2C-D) despite lower bacterial loads (Fig. 2E). We then supplemented streptomycin-treated mice with tributyrin (TB), a butyrate precursor which has been used to restore epithelial hypoxia upon streptomycin treatment(*27*, *28*). TB supplementation partially restored epithelial hypoxia (Fig. 2B) and reduced the concentration of MAIT ligands in the cecum (Fig. 2C-D). Thus, MAIT ligand production follows oxygen levels in the colon.

The oxygen-induced production of MAIT ligands can result from shifts in microbiota composition favoring the outgrowth of strong MAIT ligand producers, or from the response of individual species to oxygen. A previous study reported reduced MAIT ligand production by *E. coli* grown aerobically as compared to anaerobically(*29*). To further evaluate how oxygen exposure affects MAIT ligand production at the species level, 4 species belonging to the main intestinal Phyla (*Bacteroides thetaiotaomicron*, *E. coli*, *Clostridium perfringens* and *Clostridioides difficile*) and competent for riboflavin biosynthesis were grown anaerobically prior to exposure to air for 1h. Oxygen exposure did not induce MAIT ligand synthesis (Fig. S3C), suggesting that individual bacterial responses to oxygen may not represent a major source of MAIT ligands during dysanaerobiosis.

Intestinal inflammation triggers riboflavin and MAIT ligand production by the microbiota

Since oxygenation of the colon lumen induces shifts in microbiota composition during intestinal inflammation(*30*), we hypothesized that MAIT ligands could be overproduced by the microbiota during colitis. We used dextran salt sulfate (DSS) to induce colonic epithelium injuries and inflammation (Fig. S4A). Colitis was associated with reduced butyrate levels in the cecum (Fig. 3A) and loss of pimonidazole staining in the colon, indicating reduced epithelial hypoxia (Fig. 3B). Accordingly, MAIT ligand concentrations were increased in the cecum of DSS-treated mice (Fig. 3C), indicating overproduction of MAIT ligands by the microbiota.

We then sequenced the cecal RNA and DNA contents to better define the bacterial communities and functions associated with MAIT ligand production during colitis. Metagenomic and metatranscriptomic analyses revealed the presence of mouse DNA and RNA in the cecum lumen during colitis (Fig. 3D and S4B). The expressed genes matched granulocyte and phagocyte transcriptional signatures (Fig. 3E), suggesting that innate immune cells crossed the inflamed intestinal epithelium and were released into the lumen. We identified the up-regulated mouse and bacterial genes to determine how intestinal inflammation shaped the host-microbiota cross-talk. Multiple mouse genes involved in antibacterial defense (*Nos2*, *Lcn2*, antimicrobial peptides *S100a8*, *S100a9*), innate immune responses (*Nlrp3*, *Il1a*, *Il1b*) and oxidative stress resistance (glutathione reductase *Gsr*, *Slc7a11*, *Dusp1*) (Fig. 3F and S4C-D and Table S2a) were upregulated in the cecum lumen upon colitis, consistent with increased inflammation and oxidative stress. In response, bacterial genes involved in resistance to antimicrobial peptides and to oxidative stress (catalase-peroxidase, methionine sulfoxide reductase, catalase, cytochrome-c peroxidase among others) were upregulated in colitis (Fig. 3G, S4E and Table S2b), while genes of the butyrate metabolism were downregulated (Fig. S4F). Importantly, the genes of the riboflavin biosynthetic pathway were also upregulated in bacteria during colitis (Fig. 3G), specifically *ribBA* and *ribD*, which control 5-A-RU production (Fig. 3H). Quantification of riboflavin itself revealed increased concentrations in the cecum of DSS-treated mice as compared to control mice, well above plasma levels(*31*), confirming increased activity of this metabolic pathway in the gut during colitis (Fig. 3I).

Next, we analyzed the taxonomy of the microbiota at the DNA and RNA levels to determine microbial composition and transcriptional activity. Principal component analysis (PCA) of bacterial DNA reads clearly distinguished Mock- and DSS-treated mice (Fig. 3J), indicating significant shifts in microbiota composition induced by the treatment. Bacterial families enriched at the DNA level were usually also enriched at the RNA level, suggesting that most families were transcriptionally

active (Fig S4G). In particular, *Deferribacteres* (Family *Deferribacteraceae*) were a minor component of the microbiota at steady-state, but were enriched at the DNA and RNA level in DSS-treated mice (Fig. 3K and S4H), indicating that this Phylum was expanded and transcriptionally active during colitis, in line with earlier reports(*25*, *32*). *Enterobacteriacea*e were also enriched in DSS-treated mice at both DNA and RNA levels (Table S2c-d). We then analyzed the *ribD* transcripts to identify bacteria contributing to MAIT ligand production during colitis. While steady-state *ribD* expression was dominated by *Proteobacteria* (Family *Desulfovibrionaceae*), *ribD* was mostly expressed by *Deferribacteres* (Family *Deferribacteraceae*) during colitis (Fig. 3L and S4I). *M. schaedleri* alone contributed 47% of the *ribD* expressed in colitis (Fig. 3M), suggesting that this species is a major producer of MAIT ligands during colitis. *ribD* reads from *Bacteroides* (Family *Bacteroidaceae*) and *Verrucomicrobia* (Family *Akkermansiaceae*) were detected at the DNA (Fig. 3L and S4I), but not the RNA level, suggesting transcriptional regulation of *ribD in vivo*.

To assess the robustness of our findings, we re-analyzed a published meta-transcriptomic dataset from fecal bacteria upon *Helicobacter hepaticus*-induced colitis(*33*). Although the colitis model and sampling locations were different, the riboflavin pathway genes were also upregulated (Fig. S4J). All the genes controlling 5-A-RU production, including *ribD*, were more expressed during colitis (padj<0.01, Fig. S4J). PCA of riboflavin biosynthesis gene expression readily distinguished mice before and after colitis induction (Fig S4J), which suggests that the riboflavin biosynthesis pathway activity can be used as a colitis marker across experimental models.

MAIT ligands cross the intestinal barrier and activate MAIT cells in various tissues

MAIT ligands produced in the lumen may diffuse in the whole body as MAIT ligands can rapidly cross the mouse skin(*34*). To assess whether the intestinal epithelium was permeable to 5-OP-RU, a mixture of antigenic peptide ($OVA_{323-339}$) and 5-OP-RU metabolite was deposited into the lumen of intestinal explants from untreated mice and incubated on top of antigen-presenting cell lines (Fig. 4A). WT3-MR1 cells were used for 5-OP-RU presentation, while mutuDC cells were used for Ova presentation(*35*). After 10 min of incubation, colon explants were removed, and antigen-presenting cells were incubated with 5-OP-RU-specific- and Ova-specific TCR-Tg T cells to evaluate the presence of these ligands (Fig. 4A). 5-OP-RU-specific-, but not Ova-specific-, TCR-Tg T cells became activated (Fig. 4B), indicating rapid and efficient transfer of 5-OP-RU across the whole intestinal wall *ex vivo*. Importantly, this rapid passage of 5-OP-RU through the gut wall was observed at rather physiological dose (<= 10 pmoles in the lumen). Given the hydrophilic nature of 5-OP-RU, this result suggests the presence of an unknown transporter expressed by intestinal epithelial cells.

To test whether MAIT cells sense ligands *in vivo*, we used B6-MAIT^{Cast} mice crossed to the *Nr4a1*-GFP reporter mouse in which TCR signalling drives GFP expression(*36*). We confirmed that TCR, but not interleukin (IL)-12 and IL-18 stimulation, controls *Nr4a1*-GFP expression in MAIT cells (Fig. S5A). MAIT cells identified using the MR1:5-OP-RU tetramer (see gating strategy in Fig. S5B) represented 0.5-10% of T cells in the colonic lamina propria in B6-MAIT^{Cast} mice (Fig. 4C). At steady-state, MAIT cells expressed *Nr4a1*-GFP in the colon, mesenteric lymph nodes (mLN) and liver (Fig. S5C), consistent with low levels of ligand production in the colon and transport of these ligands through the lymph and the blood. DSS-induced colitis increased *Nr4a1*-GFP

expression in MAIT cells from the colon, but also from the mLN, liver, inguinal and brachial (I+B) LN and spleen (Fig. 4D and S5D), indicating TCR-mediated activation across peripheral tissues. By contrast, intestinal inflammation had no effect on *Nr4a1*-GFP expression in iNKT cells (Fig. 4D). Colitis was also associated with increased numbers of MAIT cells in the colon (Fig. S5E). Thus, colitis drives expression of the riboflavin pathway in the microbiota, resulting in MAIT ligand production and in MAIT cell activation.

Mice lacking MAIT cells are more susceptible to chronic colitis

TCR stimulation of MAIT cells *in vitro* triggers expression of tissue-repair mediators(*17*, *18*), including the growth factor amphiregulin (*Areg*), which induces differentiation of intestinal epithelial cells and protects against intestinal damage(*37*). To assess the effect of TCR signalling on intestinal MAIT cells *in vivo*, we generated a conditional MR1 transgenic mouse (Lox-STOP-Lox-MR1, subsequently referred to as LSL-MR1) for Cre-mediated over-expression of MR1 (Fig. S6A). The strain was validated by crossing to CD11c-Cre and confirming MR1 overexpression in dendritic cells (Fig. S6B). The LSL-MR1 mouse was then crossed to the Villin-CreER mouse for inducible expression in intestinal epithelial cells(*38*). Transgenic MR1 expression in intestinal epithelial cells had no effect on microbiota production of MAIT ligands (Fig. S6C) but elicited strong TCR signalling in MAIT cells from the colon, but not spleen and liver, as expected (Fig. 5A). Thus, the LSL-MR1 x Villin-CreER strain can help isolate the effect of TCR stimulation on colonic MAIT cells. TCR signalling in colonic MAIT cells was sufficient to induce the production of Areg *in vivo* (Fig. 5B), consistent with previous *in vitro* observations(*17, 18*) and suggesting that TCR stimulation of MAIT cells may promote epithelial repair.

To investigate the role of MAIT cells in colitis, we turned to a chronic DSS model, which mimics intestinal inflammatory flares and can provide insights into adaptive immune responses to colitis(*39*). To this end, B6-MAIT^{Cast} mice on a *Mr1*$^{+/+}$ or *Mr1*$^{-/-}$ background (hence lacking MAIT cells) were co-housed to homogenize the microbiota, and then subjected to successive cycles of DSS treatments followed by a recovery phase (Fig. S6D). At the end of the last recovery phase, MAIT cells from colitic mice spontaneously produced interferon-gamma (IFN-γ), IL-17A, IL-22 and Areg in the colon (Fig. 5C). IFN-γ promotes mucus secretion by goblet cells(*40*), while IL-17A and IL-22 stimulate secretion of anti-microbial peptides and expression of tight-junction proteins in epithelial cells(*41*), thereby reinforcing the epithelial barrier. To determine the role of MAIT cells in chronic colitis, colons from *Mr1*$^{+/+}$ and *Mr1*$^{-/-}$ mice were scored for inflammation and histopathology upon chronic DSS treatment. *Mr1*$^{-/-}$ mice experienced more severe weight loss than *Mr1*$^{+/+}$ counterparts upon chronic colitis (Fig. 5D). The presence of MAIT cells was associated with reduced inflammatory cell infiltrates, improved epithelial architecture, reduced hyperplasia (Fig. 5E) and reduced splenomegaly (Fig. S6E). Of note, the numbers of iNKT and $\gamma\delta$ T cells remained unchanged in the thymus and peripheral tissues in the absence of *Mr1* (Fig. S6F), ruling out a potential compensatory expansion of these cells in the absence of MAIT cells. Thus, MAIT cells likely protect against chronic intestinal inflammation.

Previous studies reported dysbiosis in *Mr1*$^{-/-}$ mice at steady-state(*42*), which could contribute to the observed enhanced pathology in these mice during chronic colitis. To characterize the effect of *Mr1* on the intestinal microbiota, fecal samples from co-housed, non-treated *Mr1*$^{+}$ and *Mr1*$^{-/-}$ B6-MAIT^{Cast} mice were compared by 16S rRNAseq. We could not detect any bacterial Family with

changed abundance (padj<0.01) between the two groups (Table S3a). Samples clustered together by cage of origin, rather than by mouse genotype (Fig. 5F), indicating that the microbiota was not impacted by *Mr1* at steady-state. Thus, enhanced pathology in *Mr1*$^{-/-}$ mice is likely independent of pre-existing microbiota composition. To determine whether MAIT cells affect microbiota composition upon colitis, samples from co-housed *Mr1*$^{+}$ and *Mr1*$^{-/-}$ B6-MAIT^{Cast} mice were analyzed by 16S rRNAseq after chronic colitis induction. Five bacterial Families were differentially abundant (padj<0.01) between *Mr1*$^{+}$ and *Mr1*$^{-/-}$ mice with chronic colitis (Table S3b) and mice clustered by genotype rather than by cage of origin (Fig. 5G). Interestingly, the Families *Bacteroidaceae* and *Enterobacteriacea*e, which expand during colitis (Table S2d and (*1*)), were further expanded in *Mr1*$^{-/-}$ mice as compared to *Mr1*$^{+}$ controls (Table S3b) consistent with *Mr1*$^{-/-}$ mice suffering worst colitis than *Mr1*$^{+}$ mice. Thus, the lack of MAIT cells during chronic colitis is associated with an expansion of bacterial Families such as *Enterobacteriaceae*, likely as a consequence of increased pathology.

In an attempt to demonstrate a direct protective effect of MAIT cells during colitis, we transferred *in vitro*-expanded MAIT cells into CD3$\varepsilon^{-/-}$ mice. Unexpectedly, CD3$\varepsilon^{-/-}$ mice were not protected against chronic colitis (Fig. S6G-H). This negative result does not dismiss a protective effect of MAIT cells as technical caveats are numerous: a possible modification of MAIT cells during *in vitro* expansion, a low number of cells reaching the colon or potentially incorrect localization of MAIT cells in the colon. The microbiota may also be modified in CD3$\varepsilon^{-/-}$ mice. Moreover, the protective effect of MAIT cells may rely on triggering other T cells which are lacking in CD3e$^{-/-}$ mice or may be counter-acted by an increase of other immune cells compensating for the lack of T cells. As *Mr1*$^{+}$ are less susceptible to colitis than *Mr1*$^{-/-}$ mice (Fig. 5D), this negative result could also suggest that the protective effect of MAIT cells might be indirect.

Mice lacking MAIT cells are more susceptible to inflammation-induced colorectal cancer

Chronic intestinal inflammation is a risk factor for colorectal cancer (CRC). To define the role of MAIT cells in colitis-induced CRC, colorectal tumors were induced in *Mr1*$^{+}$ and *Mr1*$^{-/-}$ B6-MAIT^{Cast} mice using the azoxymethane (AOM) + DSS model, in which administration of the carcinogen AOM is followed by three phases of DSS-induced colitis. Again, *Mr1*$^{+}$ and *Mr1*$^{-/-}$ mice were cohoused to normalize the microbiota prior to and for the duration of the experiment. Colorectal tumors were enumerated 60-80 d after the last DSS cycle (Fig. S7A). Only mice receiving both AOM and DSS developed colon tumors. *Mr1*$^{-/-}$ mice developed higher numbers of rectal tumors than *Mr1*$^{+}$ mice, strongly suggesting that MAIT cells alleviate inflammation-driven colonic tumorigenesis (Fig. 6A). The presence of colorectal tumors was not associated with increased frequencies or numbers of MAIT cells in the colon (Fig. S7B), nor with production of MAIT ligands (Fig. S7C). TCR signaling was not increased in MAIT cells from tumor-bearing mice (Fig. S7D), indicating that MAIT cells were not activated by microbiota-derived ligands at the time of euthanasia (ie 60-80 d after the last DSS cycle) in CRC-bearing mice. Furthermore, MAIT cells did not provide protection against colorectal tumor development in an orthotopic model (Fig. S7E-F), suggesting that MAIT cell protective effect in the colitis-associated CRC model was exerted by decreasing intestinal inflammation.

To define the transcriptional response of MAIT cells to chronic colitis, colonic MAIT cells from control (AOM alone) or colitic (DSS-treated) mice were FACS-sorted and analyzed by single-cell

RNAseq. After quality control and filtering, 2,903 and 2,584 MAIT cells from control and colitic mice, respectively, were retained and integrated for downstream analyses. Uniform manifold approximation and projection (UMAP) identified 13 clusters of cells (Fig 6B). Genes differentially expressed in each cell cluster were identified (Table S4) and displayed on a heatmap (Fig. S8A). Cell clusters were then labeled according to the expression of known marker genes (Fig. S8A). The analysis identified a small subset of naïve-like cells (expressing *Sell* (encoding CD62L), *Ccr7* and *Klf2*) (cluster #7) (Fig. S8A and Table S3), MAIT1 cells (expressing *Tbx21*, *Ifng* and *Ccl5*) (cluster #11) and cycling cells (expressing proliferation genes such as *Mki67*) (cluster #9) (Fig. 6C and S8A). Except for the naïve-like and MAIT1 cells, all cells expressed a MAIT17 program, which was blended with a MAIT1 program in some cells (Fig. S8B) as described elsewhere(*43*). Partition of the cells according to their origin revealed a cluster of MAIT cells uniquely present upon chronic intestinal inflammation (Fig. 6B, cluster 5) and characterized by expression of anti-inflammatory (*Tgfb1* and *Ctla4*) and cytotoxicity genes (*Gzmb, Srgn*) (Fig. 6C and S8A and Table S3). Interestingly, MAIT cells from the colitis-specific cluster were also characterized by the expression of *Il17a* and *Il22*, with well-documented beneficial effects on the intestinal epithelium during colitis(*41*, *44–46*) (Fig. 6C-D). These MAIT cells also expressed a gene signature (described in Table S5) previously associated with tissue-repair functions(*47*) (Fig. 6E). In particular, MAIT cells in colitis expressed higher levels of the transcriptional regulator *Hif1a* (Fig. 6C and Table S4), which expression protects against colitis(*48*), and *Furin* (Fig. 6C and Table S4), which encodes a convertase essential for the maturation of anti-inflammatory proproteins such as TGF-β1(*49*). Furin controls the protective function of regulatory T cells in the adoptive transfer model of colitis(*49*), suggesting that *Furin* expression by MAIT cells may contribute to their protective functions. Thus, MAIT cells in the inflamed colon express anti-inflammatory and tissue-repair genes and mice lacking MAIT cells are more susceptible to chronic colitis and colitis-induced colorectal cancer, strongly arguing for a protective role of MAIT cells against colonic inflammation.

Discussion

Microbiota-derived MAIT ligands control MAIT cell development and functions(*26*, *34*), yet the bacterial species involved, and the factors controlling MAIT ligand production in the intestinal ecosystem remained undefined. Here, we used meta-transcriptomics coupled to a sensitive bioassay to quantify MAIT ligands in distinct ecological niches of the large intestine. At steady-state, the genes of the riboflavin biosynthetic pathway were expressed by mucosa-associated bacteria, and MAIT ligands were produced in the colon mucosa. Such a production of ligands in close contact to the host may contribute to MAIT cell thymic maturation, maintenance in periphery and/or immediate functional capacities. MAIT ligands were also abundantly synthesized in the colon lumen of mice before weaning, during a developmental time-window critical for MAIT cell seeding of the skin(*26*).

Colonic hypoxia is only established at weaning, and mucosa-associated bacterial communities in adults are profoundly shaped by the oxygen emanating from the colon epithelium, suggesting a link between oxygen availability and microbiota synthesis of MAIT ligands. In line with this hypothesis, disruption of intestinal hypoxia using streptomycin treatment increased production of MAIT ligands, while restoration of hypoxia using tributyrin reduced MAIT ligand production. Exposure of individual intestinal bacterial species to oxygen did not induce MAIT ligand

production, suggesting that oxygen-induced community shifts, rather than individual bacterial responses, caused MAIT ligand production during dysanaerobiosis. Thus, oxygen may represent a key ecological factor explaining the temporally and spatially segregated production of MAIT ligands observed in the colon.

The production of MAIT ligands during dysanaerobiosis appears particularly relevant in the context of IBD, a condition associated with increased oxygen levels in the lumen(*1*, *2*). Experimental colitis was indeed associated with increased oxygen availability in the colon lumen and with the expansion of aerotolerant and facultative anaerobic bacteria. Bacterial genes involved in resistance to oxidative stress were induced by colitis, together with the genes of the riboflavin biosynthetic pathway. The analysis of a previously published meta-transcriptomic dataset from the *H. hepaticus* model of colitis confirmed over-expression of the riboflavin pathway during colitis. Increased transcription of *rib* genes translated into increased production of riboflavin and MAIT ligands upon DSS treatment.

Although 85% of all bacterial species harbor the genes encoding a full riboflavin biosynthesis pathway(*50*), only a handful of species expressed *ribD in vivo*. Intriguingly, the species expressing *ribD* belonged to minor components of the microbiota, primarily from the Phyla *Proteobacteria* and *Deferribacteres*. Moreover, the increased transcription of *ribD* in mucosa and during colitis was mainly driven by a single species (*M. schaedleri*), which resided in mucosa at steady-state and bloomed during inflammation. These observations support the hypothesis that MAIT ligands are primarily produced by expanded aerotolerant bacteria during dysanaerobiosis. Further studies are necessary to quantify MAIT ligand synthesis by the individual bacterial species identified as *ribD* expressors and to determine how this synthesis impacts the host immune system. *M. schaedleri* can trigger colitis in immunodeficient hosts(*51*), but also impart protection against *Salmonella* infections(*52*). Whether these functions involve the antigen-driven activation of MAIT cells remains to be determined.

MAIT cells are located at strategic locations to detect changes in the production of MAIT ligands in the gut, in particular in the lamina propria and in the liver. Although MAIT cells display a number of receptors for cytokines such as IL-1, IL-12, IL-23, and IFNγ(*53*), MAIT cells were activated through the TCR during DSS-induced colitis. Thus, the emerging picture is that MAIT cells monitor the microbiota shifts that are induced with colitis (Fig. 6F). Given the ability of MAIT ligands to rapidly cross the intestinal epithelium, MAIT cells may detect the earliest events of dysbiosis and provide an immediate effector response. Intriguingly, colitis triggered TCR signaling in MAIT cells from all the studied tissues, including non-gut draining lymph nodes, consistent with the ability of 5-OP-RU to travel across the body. MAIT cell activation in distant tissues may represent a systemic surveillance strategy of intestinal inflammation, the implications of which remain to be investigated. Since MAIT cell transcriptional features are shaped by their tissue of residence(*53*), body-wide TCR activation as seen during colitis may result in local production of mediators tuned to each tissue(*54*). The activation of distant MAIT cells may also induce trafficking to the gut, which could explain the increased MAIT cell numbers in the inflamed colon.

Future work should address whether dysanaerobiosis similarly drives MAIT ligand production by the human intestinal microbiota. Mucosa-associated microbiota in humans, like in mice, are

enriched in *Proteobacteria* and aerotolerant species(*22*), including *M. schaedleri*(*52*), suggesting that MAIT ligands may be abundantly synthesized in human mucosa as well. The riboflavin biosynthesis pathway is found more frequently in microbiota from a subset of IBD patients(*14*), in line with our observation of increased riboflavin synthesis in experimental colitis.

MAIT cells can exert pro- or anti-inflammatory responses depending on the context. In IBD patients, several groups observed decreased MAIT cell frequencies in blood coupled with activation and recruitment of MAIT cells in inflamed lesions(*9*, *10*) which correlated with disease activity(*10*, *55*). Because MAIT cells produce cytokines that can be either deleterious (TNFα) or beneficial (IL-17A and IL-22) in IBD patients, their role in the progression of the disease was unclear in absence of experimental manipulation. Our data establish that the presence of MAIT cells is associated with reduced intestinal epithelial damage during chronic colitis and reduced development of colitis-associated colorectal tumors. Chronic colitis induced the expression of a tissue-repair transcriptional program in MAIT cells, in good agreement with the proposed link between MAIT cell TCR stimulation and tissue-repair functions(*17*, *18*). In particular, MAIT cells produced amphiregulin in the colon upon TCR engagement and during chronic inflammation. MAIT cell-derived amphiregulin accelerates the skin healing process(*56*), suggesting a potentially similar mechanism in the gut upon epithelial damage. In addition to tissue-repair mediators, MAIT cells produced IL-17A and IL-22 during colitis. IL-17A stimulates occludine expression in the intestinal epithelium, directly strengthening tight junctions and reducing intestinal permeability(*44*, *45*). IL-22 promotes the intestinal barrier through the induction of mucus and antimicrobial peptide secretion(*46*, *57*, *58*). IL-22 also sustains intestinal epithelial stem cell survival and epithelium repair upon injury(*59*). Thus, MAIT cells produce an array of effector molecules with barrier-promoting effects during intestinal epithelial damage and inflammation. These results are in line with previous studies reporting weakened intestinal barrier function in *Mr1*$^{-/-}$ mice(*42*, *60*), and support a key role for MAIT cells in promoting epithelial barrier integrity. The exact contribution of each MAIT-derived effector molecule remains to be determined. Of note, our results contradict a previous study reporting worse pathology in *Mr1*$^{+/+}$ mice as compared to *Mr1*$^{-/-}$ mice in the oxazolone model of colitis, in which inflammation is triggered by immunization against microbiota antigens(*61*). The apparent discrepancy may derive from the models used (acute in the case of oxazolone colitis *versus* chronic in our model). In addition, interpretation of the results from Yasutomi et al is complicated by the use of a lower oxazolone dose for some of the control mice, which were more susceptible to colitis because they originated from commercial vendors (while *Mr1*$^{-/-}$ mice were produced in-house)(*61*). Thus, colitis severity in that study may be primarily determined by the microbiota instead of by MAIT cells.

In humans, MAIT cell frequencies are modified in the blood of patients with obesity(*62*) and diabetes(*60*), conditions in which the microbiota is modified. Whether dysbiosis in these diseases is associated with TCR-dependent activation of MAIT cells remains to be addressed. Notably, MAIT cells seem to preserve the integrity of the meningeal barrier and cognitive brain function in mice(*63*). The role of microbiota-derived MAIT ligands in MAIT cell functions in the brain remains to be determined.

In conclusion, we highlight a new function of MAIT cells in the colon: monitoring the activity of a microbial metabolic pathway indicative of intestinal inflammation to provide anti-inflammatory and tissue-repair mediators in return.

Supplementary Materials

Materials and methods
Fig. S1: Bacterial production of MAIT antigens in the colonic mucosa.
Fig. S2: Bacterial gene expression in lumen and mucosa.
Fig. S3: MAIT ligand production upon bacterial exposure to air.
Fig. S4: Bacterial gene expression in response to DSS-induced colitis.
Fig. S5: Nur77 expression in MAIT cells at steady-state and upon DSS-induced colitis.
Fig. S6: *Mr1*$^{-/-}$ mice are more sensitive to chronic DSS-induced colitis.
Fig. S7: *Mr1*$^{-/-}$ mice develop more rectal tumors in the AOM/DSS colitis-induced colorectal tumor model.
Fig. S8: Gene expression in colonic MAIT cells upon colitis.
Table S1: DESeq2 results upon comparison of bacterial counts (based on 16S rRNA gene sequencing) between colon mucosa and lumen.
Table S2: DESeq2 results upon comparison of metatranscriptomic reads between untreated and DSS-treated mice.
Table S3: DESeq2 results upon comparison of bacterial read counts (based on 16S rRNA gene sequencing) between co-housed Mr1+ and Mr1-/- mice at steady-state and upon chronic colitis induction.
Table S4: Genes identified as differentially expressed in UMAP clusters from colonic MAIT cells.
Table S5: Tissue-repair gene signature from Linehan et al, Cell 2018
Table S6: Antibodies and reagents used in the study.

References and Notes

1. J.-Y. Lee, R. M. Tsolis, A. J. Bäumler, The microbiome and gut homeostasis. *Science* **377**, eabp9960 (2022).

2. Y. Litvak, M. X. Byndloss, A. J. Bäumler, Colonocyte metabolism shapes the gut microbiota. *Science* **362**, eaat9076 (2018).

3. M. X. Byndloss, A. J. Bäumler, The germ-organ theory of non-communicable diseases. *Nat. Rev. Microbiol.* **16**, 103–110 (2018).

4. F. Legoux, M. Salou, O. Lantz, MAIT Cell Development and Functions: the Microbial Connection. *Immunity* **53**, 710–723 (2020).

5. A. J. Corbett, S. B. G. Eckle, R. W. Birkinshaw, L. Liu, O. Patel, J. Mahony, Z. Chen, R. Reantragoon, B. Meehan, H. Cao, N. A. Williamson, R. A. Strugnell, D. Van Sinderen, J. Y. W. Mak, D. P. Fairlie, L. Kjer-Nielsen, J. Rossjohn, J. McCluskey, T-cell activation by transitory neo-antigens derived from distinct microbial pathways. *Nature* **509**, 361–365 (2014).

6. C. Soudais, F. Samassa, M. Sarkis, L. Le Bourhis, S. Bessoles, D. Blanot, M. Hervé, F. Schmidt, D. Mengin-Lecreulx, O. Lantz, In Vitro and In Vivo Analysis of the Gram-Negative Bacteria-Derived Riboflavin Precursor Derivatives Activating Mouse MAIT Cells. *J. Immunol. Baltim. Md 1950* **194**, 4641–4649 (2015).

7. C. Tastan, E. Karhan, W. Zhou, E. Fleming, A. Y. Voigt, X. Yao, L. Wang, M. Horne, L. Placek, L. Kozhaya, J. Oh, D. Unutmaz, Tuning of human MAIT cell activation by commensal bacteria species and MR1-dependent T-cell presentation. *Mucosal Immunol.* **11**, 1591–1605 (2018).

8. H. J. Kim, D. R. Winge, Emerging concepts in the flavinylation of succinate dehydrogenase. *Biochim. Biophys. Acta* **1827**, 627–636 (2013).

9. N.-E. Serriari, M. Eoche, L. Lamotte, J. Lion, M. Fumery, P. Marcelo, D. Chatelain, A. Barre, E. Nguyen-Khac, O. Lantz, J.-L. Dupas, E. Treiner, Innate mucosal-associated invariant T (MAIT) cells are activated in inflammatory bowel diseases. *Clin. Exp. Immunol.* **176**, 266–274 (2014).

10. K. Haga, A. Chiba, T. Shibuya, T. Osada, D. Ishikawa, T. Kodani, O. Nomura, S. Watanabe, S. Miyake, MAIT cells are activated and accumulated in the inflamed mucosa of ulcerative colitis: MAIT cell reflects mucosal inflammation. *J. Gastroenterol. Hepatol.* **31**, 965–972 (2016).

11. L. Ling, Y. Lin, W. Zheng, S. Hong, X. Tang, P. Zhao, M. Li, J. Ni, C. Li, L. Wang, Y. Jiang, Circulating and tumor-infiltrating mucosal associated invariant T (MAIT) cells in colorectal cancer patients. *Sci. Rep.* **6**, 20358 (2016).

12. L. Zabijak, C. Attencourt, C. Guignant, D. Chatelain, P. Marcelo, J.-P. Marolleau, E. Treiner, Increased tumor infiltration by mucosal-associated invariant T cells correlates with poor survival in colorectal cancer patients. *Cancer Immunol. Immunother. CII* **64**, 1601–1608 (2015).

13. S. Li, Y. Simoni, E. Becht, C. Y. Loh, N. Li, D. Lachance, S.-L. Koo, T. P. Lim, E. K. W. Tan, R. Mathew, A. Nguyen, J. Golovato, J. D. Berkson, M. Prlic, B. Lee, S. S. Minot, N. Nagarajan, N. Dey, D. S. W. Tan, I. B. Tan, E. W. Newell, Human Tumor-Infiltrating MAIT Cells Display Hallmarks of Bacterial Antigen Recognition in Colorectal Cancer. *Cell Rep. Med.* **1**, 100039 (2020).

14. X. C. Morgan, T. L. Tickle, H. Sokol, D. Gevers, K. L. Devaney, D. V. Ward, J. A. Reyes, S. A. Shah, N. LeLeiko, S. B. Snapper, A. Bousvaros, J. Korzenik, B. E. Sands, R. J. Xavier, C. Huttenhower, Dysfunction of the intestinal microbiome in inflammatory bowel disease and treatment. *Genome Biol.* **13**, R79 (2012).

15. D. Gevers, S. Kugathasan, L. A. Denson, Y. Vázquez-Baeza, W. Van Treuren, B. Ren, E. Schwager, D. Knights, S. J. Song, M. Yassour, X. C. Morgan, A. D. Kostic, C. Luo, A. González, D. McDonald, Y. Haberman, T. Walters, S. Baker, J. Rosh, M. Stephens, M. Heyman, J. Markowitz, R. Baldassano, A. Griffiths, F. Sylvester, D. Mack, S. Kim, W. Crandall, J. Hyams, C. Huttenhower, R. Knight, R. J. Xavier, The treatment-naive microbiome in new-onset Crohn's disease. *Cell Host Microbe* **15**, 382–392 (2014).

16. Q. Feng, S. Liang, H. Jia, A. Stadlmayr, L. Tang, Z. Lan, D. Zhang, H. Xia, X. Xu, Z. Jie, L. Su, X. Li, X. Li, J. Li, L. Xiao, U. Huber-Schönauer, D. Niederseer, X. Xu, J. Y. Al-Aama, H. Yang, J. Wang, K. Kristiansen, M. Arumugam, H. Tilg, C. Datz, J. Wang, Gut microbiome development along the colorectal adenoma-carcinoma sequence. *Nat. Commun.* **6**, 6528 (2015).

17. T. Leng, H. D. Akther, C.-P. Hackstein, K. Powell, T. King, M. Friedrich, Z. Christoforidou, S. McCuaig, M. Neyazi, C. V. Arancibia-Cárcamo, J. Hagel, F. Powrie, Oxford IBD Investigators, R. S. Peres, V. Millar, D. Ebner, R. Lamichhane, J. Ussher, T. S. C. Hinks, E. Marchi, C. Willberg, P. Klenerman, TCR and Inflammatory Signals Tune Human MAIT Cells to Exert Specific Tissue Repair and Effector Functions. *Cell Rep.* **28**, 3077-3091.e5 (2019).

18. T. S. C. Hinks, E. Marchi, M. Jabeen, M. Olshansky, A. Kurioka, T. J. Pediongco, B. S. Meehan, L. Kostenko, S. J. Turner, A. J. Corbett, Z. Chen, P. Klenerman, J. McCluskey, Activation and In Vivo Evolution of the MAIT Cell Transcriptome in Mice and Humans Reveals Tissue Repair Functionality. *Cell Rep.* **28**, 3249-3262.e5 (2019).

19. E. Martin, E. Treiner, L. Duban, L. Guerri, H. Laude, C. Toly, V. Premel, A. Devys, I. C. Moura, F. Tilloy, S. Cherif, G. Vera, S. Latour, C. Soudais, O. Lantz, Stepwise development of MAIT cells in mouse and human. *PLoS Biol.* **7**, e54 (2009).

20. S. Huang, E. Martin, S. Kim, L. Yu, C. Soudais, D. H. Fremont, O. Lantz, T. H. Hansen, MR1 antigen presentation to mucosal-associated invariant T cells was highly conserved in evolution. *Proc. Natl. Acad. Sci. U. S. A.* **106**, 8290–8295 (2009).

21. G. P. Donaldson, S. M. Lee, S. K. Mazmanian, Gut biogeography of the bacterial microbiota. *Nat. Rev. Microbiol.* **14**, 20–32 (2016).

22. L. Albenberg, T. V. Esipova, C. P. Judge, K. Bittinger, J. Chen, A. Laughlin, S. Grunberg, R. N. Baldassano, J. D. Lewis, H. Li, S. R. Thom, F. D. Bushman, S. A. Vinogradov, G. D. Wu, Correlation between intraluminal oxygen gradient and radial partitioning of intestinal microbiota. *Gastroenterology* **147**, 1055-1063.e8 (2014).

23. G. M. Douglas, V. J. Maffei, J. R. Zaneveld, S. N. Yurgel, J. R. Brown, C. M. Taylor, C. Huttenhower, M. G. I. Langille, PICRUSt2 for prediction of metagenome functions. *Nat. Biotechnol.* **38**, 685–688 (2020).

24. A. Zaborin, B. Penalver Bernabe, R. Keskey, N. Sangwan, S. Hyoju, N. Gottel, J. A. Gilbert, O. Zaborina, J. C. Alverdy, Spatial Compartmentalization of the Microbiome between the Lumen and Crypts Is Lost in the Murine Cecum following the Process of Surgery, Including Overnight Fasting and Exposure to Antibiotics. *mSystems* **5**, e00377-20 (2020).

25. A. Loy, C. Pfann, M. Steinberger, B. Hanson, S. Herp, S. Brugiroux, J. C. Gomes Neto, M. V. Boekschoten, C. Schwab, T. Urich, A. E. Ramer-Tait, T. Rattei, B. Stecher, D. Berry, Lifestyle and Horizontal Gene Transfer-Mediated Evolution of Mucispirillum schaedleri, a Core Member of the Murine Gut Microbiota. *mSystems* **2**, e00171-16 (2017).

26. M. G. Constantinides, V. M. Link, S. Tamoutounour, A. C. Wong, P. J. Perez-Chaparro, S.-J. Han, Y. E. Chen, K. Li, S. Farhat, A. Weckel, S. R. Krishnamurthy, I. Vujkovic-Cvijin, J. L. Linehan, N. Bouladoux, E. D. Merrill, S. Roy, D. J. Cua, E. J. Adams, A. Bhandoola, T. C. Scharschmidt, J. Aubé, M. A. Fischbach, Y. Belkaid, MAIT cells are imprinted by the microbiota in early life and promote tissue repair. *Science* **366** (2019).

27. F. Rivera-Chávez, L. F. Zhang, F. Faber, C. A. Lopez, M. X. Byndloss, E. E. Olsan, G. Xu, E. M. Velazquez, C. B. Lebrilla, S. E. Winter, A. J. Bäumler, Depletion of Butyrate-Producing Clostridia from the Gut Microbiota Drives an Aerobic Luminal Expansion of Salmonella. *Cell Host Microbe* **19**, 443–454 (2016).

28. C. J. Kelly, L. Zheng, E. L. Campbell, B. Saeedi, C. C. Scholz, A. J. Bayless, K. E. Wilson, L. E. Glover, D. J. Kominsky, A. Magnuson, T. L. Weir, S. F. Ehrentraut, C. Pickel, K. A. Kuhn, J. M. Lanis, V. Nguyen, C. T. Taylor, S. P. Colgan, Crosstalk between Microbiota-Derived Short-Chain Fatty Acids and Intestinal Epithelial HIF Augments Tissue Barrier Function. *Cell Host Microbe* **17**, 662–671 (2015).

29. M. Schmaler, A. Colone, J. Spagnuolo, M. Zimmermann, M. Lepore, A. Kalinichenko, S. Bhatia, F. Cottier, T. Rutishauser, N. Pavelka, A. Egli, E. Azzali, M. Pieroni, G. Costantino, P. Hruz, U. Sauer, L. Mori, G. De Libero, Modulation of bacterial metabolism by the microenvironment controls MAIT cell stimulation. *Mucosal Immunol.* **11**, 1060–1070 (2018).

30. L. Rigottier-Gois, Dysbiosis in inflammatory bowel diseases: the oxygen hypothesis. *ISME J.* **7**, 1256–1261 (2013).

31. H. Yoshimatsu, A. Yonezawa, K. Yamanishi, Y. Yao, K. Sugano, S. Nakagawa, S. Imai, T. Omura, T. Nakagawa, I. Yano, S. Masuda, K. Inui, K. Matsubara, Disruption of Slc52a3 gene causes neonatal lethality with riboflavin deficiency in mice. *Sci. Rep.* **6**, 27557 (2016).

32. C. Hoffmann, D. A. Hill, N. Minkah, T. Kirn, A. Troy, D. Artis, F. Bushman, Community-Wide Response of the Gut Microbiota to Enteropathogenic *Citrobacter rodentium* Infection Revealed by Deep Sequencing. *Infect. Immun.* **77**, 4668–4678 (2009).

33. N. E. Ilott, J. Bollrath, C. Danne, C. Schiering, M. Shale, K. Adelmann, T. Krausgruber, A. Heger, D. Sims, F. Powrie, Defining the microbial transcriptional response to colitis through integrated host and microbiome profiling. *ISME J.* **10**, 2389–2404 (2016).

34. F. Legoux, D. Bellet, C. Daviaud, Y. El Morr, A. Darbois, K. Niort, E. Procopio, M. Salou, J. Gilet, B. Ryffel, A. Balvay, A. Foussier, M. Sarkis, A. El Marjou, F. Schmidt, S. Rabot, O. Lantz, Microbial metabolites control the thymic development of mucosal-associated invariant T cells. *Science*, doi: 10.1126/science.aaw2719 (2019).

35. S. A. Fuertes Marraco, F. Grosjean, A. Duval, M. Rosa, C. Lavanchy, D. Ashok, S. Haller, L. A. Otten, Q.-G. Steiner, P. Descombes, C. A. Luber, F. Meissner, M. Mann, L. Szeles, W. Reith, H. Acha-Orbea, Novel murine dendritic cell lines: a powerful auxiliary tool for dendritic cell research. *Front. Immunol.* **3**, 331 (2012).

36. J. Zikherman, R. Parameswaran, A. Weiss, Endogenous antigen tunes the responsiveness of naive B cells but not T cells. *Nature* **489**, 160–164 (2012).

37. L. A. Monticelli, L. C. Osborne, M. Noti, S. V. Tran, D. M. W. Zaiss, D. Artis, IL-33 promotes an innate immune pathway of intestinal tissue protection dependent on amphiregulin-EGFR interactions. *Proc. Natl. Acad. Sci. U. S. A.* **112**, 10762–10767 (2015).

38. F. el Marjou, K.-P. Janssen, B. H.-J. Chang, M. Li, V. Hindie, L. Chan, D. Louvard, P. Chambon, D. Metzger, S. Robine, Tissue-specific and inducible Cre-mediated recombination in the gut epithelium. *Genes. N. Y. N 2000* **39**, 186–193 (2004).

39. S. Wirtz, V. Popp, M. Kindermann, K. Gerlach, B. Weigmann, S. Fichtner-Feigl, M. F. Neurath, Chemically induced mouse models of acute and chronic intestinal inflammation. *Nat. Protoc.* **12**, 1295–1309 (2017).

40. C. S. N. Klose, E. A. Kiss, V. Schwierzeck, K. Ebert, T. Hoyler, Y. d'Hargues, N. Göppert, A. L. Croxford, A. Waisman, Y. Tanriver, A. Diefenbach, A T-bet gradient controls the fate and function of CCR6-RORγt+ innate lymphoid cells. *Nature* **494**, 261–265 (2013).

41. S. C. Liang, X.-Y. Tan, D. P. Luxenberg, R. Karim, K. Dunussi-Joannopoulos, M. Collins, L. A. Fouser, Interleukin (IL)-22 and IL-17 are coexpressed by Th17 cells and cooperatively enhance expression of antimicrobial peptides. *J. Exp. Med.* **203**, 2271–2279 (2006).

42. A. Varelias, M. D. Bunting, K. L. Ormerod, M. Koyama, S. D. Olver, J. Straube, R. D. Kuns, R. J. Robb, A. S. Henden, L. Cooper, N. Lachner, K. H. Gartlan, O. Lantz, L. Kjer-Nielsen, J. Y. W. Mak, D. P. Fairlie, A. D. Clouston, J. McCluskey, J. Rossjohn, S. W. Lane, P. Hugenholtz, G. R. Hill, Recipient mucosal-associated invariant T cells control GVHD within the colon. *J. Clin. Invest.* **128**, 1919–1936 (2018).

43. H. Bugaut, Y. El Morr, M. Mestdagh, A. Darbois, R. A. Paiva, M. Salou, L. Perrin, M. Fürstenheim, A. du Halgouet, L. Bilonda-Mutala, A.-L. Le Gac, M. Arnaud, A. El Marjou, C. Guerin, A. Chaiyasitdhi, J. Piquet, D. M. Smadja, A. Cieslak, B. Ryffel, V. Maciulyte, J. M. A. Turner, K. Bernardeau, X. Montagutelli, O. Lantz, F. Legoux, A conserved transcriptional program for MAIT cells across mammalian evolution. *J. Exp. Med.* **221**, e20231487 (2024).

44. J. S. Lee, C. M. Tato, B. Joyce-Shaikh, M. F. Gulen, C. Cayatte, Y. Chen, W. M. Blumenschein, M. Judo, G. Ayanoglu, T. K. McClanahan, X. Li, D. J. Cua, Interleukin-23-Independent IL-17 Production Regulates Intestinal Epithelial Permeability. *Immunity* **43**, 727–738 (2015).

45. X. Song, D. Dai, X. He, S. Zhu, Y. Yao, H. Gao, J. Wang, F. Qu, J. Qiu, H. Wang, X. Li, N. Shen, Y. Qian, Growth Factor FGF2 Cooperates with Interleukin-17 to Repair Intestinal Epithelial Damage. *Immunity* **43**, 488–501 (2015).

46. K. Sugimoto, A. Ogawa, E. Mizoguchi, Y. Shimomura, A. Andoh, A. K. Bhan, R. S. Blumberg, R. J. Xavier, A. Mizoguchi, IL-22 ameliorates intestinal inflammation in a mouse model of ulcerative colitis. *J. Clin. Invest.*, JCI33194 (2008).

47. J. L. Linehan, O. J. Harrison, S.-J. Han, A. L. Byrd, I. Vujkovic-Cvijin, A. V. Villarino, S. K. Sen, J. Shaik, M. Smelkinson, S. Tamoutounour, N. Collins, N. Bouladoux, A. Dzutsev, S. P. Rosshart, J. H. Arbuckle, C.-R. Wang, T. M. Kristie, B. Rehermann, G. Trinchieri, J. M. Brenchley, J. J. O'Shea, Y. Belkaid, Non-classical Immunity Controls Microbiota Impact on Skin Immunity and Tissue Repair. *Cell* **172**, 784-796.e18 (2018).

48. J. Karhausen, G. T. Furuta, J. E. Tomaszewski, R. S. Johnson, S. P. Colgan, V. H. Haase, Epithelial hypoxia-inducible factor-1 is protective in murine experimental colitis. *J. Clin. Invest.* **114**, 1098–1106 (2004).

49. M. Pesu, W. T. Watford, L. Wei, L. Xu, I. Fuss, W. Strober, J. Andersson, E. M. Shevach, M. Quezado, N. Bouladoux, A. Roebroek, Y. Belkaid, J. Creemers, J. J. O'Shea, T-cell-expressed proprotein convertase furin is essential for maintenance of peripheral immune tolerance. *Nature* **455**, 246–250 (2008).

50. S. Mondot, P. Boudinot, O. Lantz, MAIT, MR1, microbes and riboflavin: a paradigm for the co-evolution of invariant TCRs and restricting MHCI-like molecules? *Immunogenetics* **68**, 537–548 (2016).

51. R. Caruso, T. Mathes, E. C. Martens, N. Kamada, A. Nusrat, N. Inohara, G. Núñez, A specific gene-microbe interaction drives the development of Crohn's disease-like colitis in mice. *Sci. Immunol.* **4**, eaaw4341 (2019).

52. S. Herp, S. Brugiroux, D. Garzetti, D. Ring, L. M. Jochum, M. Beutler, C. Eberl, S. Hussain, S. Walter, R. G. Gerlach, H. J. Ruscheweyh, D. Huson, M. E. Sellin, E. Slack, B. Hanson, A. Loy, J. F. Baines, P. Rausch, M. Basic, A. Bleich, D. Berry, B. Stecher, Mucispirillum schaedleri Antagonizes Salmonella Virulence to Protect Mice against Colitis. *Cell Host Microbe* **25**, 681-694.e8 (2019).

53. M. Salou, F. Legoux, J. Gilet, A. Darbois, A. du Halgouet, R. Alonso, W. Richer, A.-G. Goubet, C. Daviaud, L. Menger, E. Procopio, V. Premel, O. Lantz, A common transcriptomic program acquired in the thymus defines tissue residency of MAIT and NKT subsets. *J. Exp. Med.*, doi: 10.1084/jem.20181483 (2018).

54. M. A. Ataide, K. Knöpper, P. Cruz de Casas, M. Ugur, S. Eickhoff, M. Zou, H. Shaikh, A. Trivedi, A. Grafen, T. Yang, I. Prinz, K. Ohlsen, M. Gomez de Agüero, A. Beilhack, J. Huehn, M. Gaya, A.-E. Saliba, G. Gasteiger, W. Kastenmüller, Lymphatic migration of unconventional T cells promotes site-specific immunity in distinct lymph nodes. *Immunity* **55**, 1813-1828.e9 (2022).

55. K. Tominaga, S. Yamagiwa, T. Setsu, N. Kimura, H. Honda, H. Kamimura, Y. Honda, M. Takamura, J. Yokoyama, K. Suzuki, T. Wakai, S. Terai, Possible involvement of mucosal-associated invariant T cells in the progression of inflammatory bowel diseases. *Biomed. Res. Tokyo Jpn.* **38**, 111–121 (2017).

56. A. du Halgouet, A. Darbois, M. Alkobtawi, M. Mestdagh, A. Alphonse, V. Premel, T. Yvorra, L. Colombeau, R. Rodriguez, D. Zaiss, Y. El Morr, H. Bugaut, F. Legoux, L. Perrin, S. Aractingi, R. Golub, O. Lantz, M. Salou, Role of MR1-driven signals and amphiregulin on the recruitment and repair function of MAIT cells during skin wound healing. *Immunity* **56**, 78-92.e6 (2023).

57. S. J. Aujla, Y. R. Chan, M. Zheng, M. Fei, D. J. Askew, D. A. Pociask, T. A. Reinhart, F. McAllister, J. Edeal, K. Gaus, S. Husain, J. L. Kreindler, P. J. Dubin, J. M. Pilewski, M. M. Myerburg, C. A. Mason, Y. Iwakura, J. K. Kolls, IL-22 mediates mucosal host defense against Gram-negative bacterial pneumonia. *Nat. Med.* **14**, 275–281 (2008).

58. Y. Zheng, P. A. Valdez, D. M. Danilenko, Y. Hu, S. M. Sa, Q. Gong, A. R. Abbas, Z. Modrusan, N. Ghilardi, F. J. de Sauvage, W. Ouyang, Interleukin-22 mediates early host defense against attaching and effacing bacterial pathogens. *Nat. Med.* **14**, 282–289 (2008).

59. C. A. Lindemans, M. Calafiore, A. M. Mertelsmann, M. H. O'Connor, J. A. Dudakov, R. R. Jenq, E. Velardi, L. F. Young, O. M. Smith, G. Lawrence, J. A. Ivanov, Y.-Y. Fu, S. Takashima, G. Hua, M. L. Martin, K. P. O'Rourke, Y.-H. Lo, M. Mokry, M. Romera-Hernandez, T. Cupedo, L. Dow, E. E. Nieuwenhuis, N. F. Shroyer, C. Liu, R. Kolesnick, M. R. M. van den Brink, A. M. Hanash, Interleukin-22 promotes intestinal-stem-cell-mediated epithelial regeneration. *Nature* **528**, 560–564 (2015).

60. O. Rouxel, J. Da Silva, L. Beaudoin, I. Nel, C. Tard, L. Cagninacci, B. Kiaf, M. Oshima, M. Diedisheim, M. Salou, A. Corbett, J. Rossjohn, J. McCluskey, R. Scharfmann, M. Battaglia, M. Polak, O. Lantz, J. Beltrand, A. Lehuen, Cytotoxic and regulatory roles of

mucosal-associated invariant T cells in type 1 diabetes. *Nat. Immunol.* **18**, 1321–1331 (2017).

61. Y. Yasutomi, A. Chiba, K. Haga, G. Murayama, A. Makiyama, T. Kuga, M. Watanabe, R. Okamoto, A. Nagahara, T. Nagaishi, S. Miyake, Activated Mucosal-associated Invariant T Cells Have a Pathogenic Role in a Murine Model of Inflammatory Bowel Disease. *Cell. Mol. Gastroenterol. Hepatol.* **13**, 81–93 (2022).

62. I. Magalhaes, K. Pingris, C. Poitou, S. Bessoles, N. Venteclef, B. Kiaf, L. Beaudoin, J. Da Silva, O. Allatif, J. Rossjohn, L. Kjer-Nielsen, J. McCluskey, S. Ledoux, L. Genser, A. Torcivia, C. Soudais, O. Lantz, C. Boitard, J. Aron-Wisnewsky, E. Larger, K. Clément, A. Lehuen, Mucosal-associated invariant T cell alterations in obese and type 2 diabetic patients. *J. Clin. Invest.* **125**, 1752–1762 (2015).

63. Y. Zhang, J. T. Bailey, E. Xu, K. Singh, M. Lavaert, V. M. Link, S. D'Souza, A. Hafiz, J. Cao, G. Cao, D. B. Sant'Angelo, W. Sun, Y. Belkaid, A. Bhandoola, D. B. McGavern, Q. Yang, Mucosal-associated invariant T cells restrict reactive oxidative damage and preserve meningeal barrier integrity and cognitive function. *Nat. Immunol.* **23**, 1714–1725 (2022).

64. Y. Cui, K. Franciszkiewicz, Y. K. Mburu, S. Mondot, L. Le Bourhis, V. Premel, E. Martin, A. Kachaner, L. Duban, M. A. Ingersoll, S. Rabot, J. Jaubert, J.-P. De Villartay, C. Soudais, O. Lantz, Mucosal-associated invariant T cell-rich congenic mouse strain allows functional evaluation. *J. Clin. Invest.* **125**, 4171–4185 (2015).

65. M. J. Barnden, J. Allison, W. R. Heath, F. R. Carbone, Defective TCR expression in transgenic mice constructed using cDNA-based alpha- and beta-chain genes under the control of heterologous regulatory elements. *Immunol. Cell Biol.* **76**, 34–40 (1998).

66. Z. Zhang, F. P. Legoux, S. W. Vaughan, J. J. Moon, Opposing peripheral fates of tissue-restricted self antigen-specific conventional and regulatory CD4+ T cells. *Eur. J. Immunol.* **50**, 63–72 (2020).

67. M. L. Caton, M. R. Smith-Raska, B. Reizis, Notch-RBP-J signaling controls the homeostasis of CD8- dendritic cells in the spleen. *J. Exp. Med.* **204**, 1653–1664 (2007).

68. T. Tanaka, H. Kohno, R. Suzuki, Y. Yamada, S. Sugie, H. Mori, A novel inflammation-related mouse colon carcinogenesis model induced by azoxymethane and dextran sodium sulfate. *Cancer Sci.* **94**, 965–973 (2003).

69. T. Yvorra, A. Steinmetz, P. Retailleau, O. Lantz, F. Schmidt, Synthesis, biological evaluation and molecular modelling of new potent clickable analogues of 5-OP-RU for their use as chemical probes for the study of MAIT cell biology. *Eur. J. Med. Chem.* **211**, 113066 (2021).

70. J. J. Kozich, S. L. Westcott, N. T. Baxter, S. K. Highlander, P. D. Schloss, Development of a dual-index sequencing strategy and curation pipeline for analyzing amplicon sequence data on the MiSeq Illumina sequencing platform. *Appl. Environ. Microbiol.* **79**, 5112–5120 (2013).

71. M. Martin, Cutadapt removes adapter sequences from high-throughput sequencing reads. *EMBnet.journal* **17**, 10 (2011).

72. N. Segata, J. Izard, L. Waldron, D. Gevers, L. Miropolsky, W. S. Garrett, C. Huttenhower, Metagenomic biomarker discovery and explanation. *Genome Biol.* **12**, R60 (2011).

73. A. Dobin, C. A. Davis, F. Schlesinger, J. Drenkow, C. Zaleski, S. Jha, P. Batut, M. Chaisson, T. R. Gingeras, STAR: ultrafast universal RNA-seq aligner. *Bioinforma. Oxf. Engl.* **29**, 15–21 (2013).

74. E. Kopylova, L. Noé, H. Touzet, SortMeRNA: fast and accurate filtering of ribosomal RNAs in metatranscriptomic data. *Bioinforma. Oxf. Engl.* **28**, 3211–3217 (2012).

75. T. R. Lesker, A. C. Durairaj, E. J. C. Gálvez, I. Lagkouvardos, J. F. Baines, T. Clavel, A. Sczyrba, A. C. McHardy, T. Strowig, An Integrated Metagenome Catalog Reveals New Insights into the Murine Gut Microbiome. *Cell Rep.* **30**, 2909-2922.e6 (2020).

76. Y. Liao, G. K. Smyth, W. Shi, featureCounts: an efficient general purpose program for assigning sequence reads to genomic features. *Bioinforma. Oxf. Engl.* **30**, 923–930 (2014).

77. M. I. Love, W. Huber, S. Anders, Moderated estimation of fold change and dispersion for RNA-seq data with DESeq2. *Genome Biol.* **15**, 550 (2014).

78. C. Nonnenmacher, A. Dalpke, R. Mutters, K. Heeg, Quantitative detection of periodontopathogens by real-time PCR. *J. Microbiol. Methods* **59**, 117–125 (2004).

79. A. Lan, A. Bruneau, C. Philippe, V. Rochet, A. Rouault, C. Hervé, N. Roland, S. Rabot, G. Jan, Survival and metabolic activity of selected strains of Propionibacterium freudenreichii in the gastrointestinal tract of human microbiota-associated rats. *Br. J. Nutr.* **97**, 714–724 (2007).

80. A. Lopez-Anaya, M. Mayersohn, Quantification of riboflavin, riboflavin 5′-phosphate and flavin adenine dinucleotide in plasma and urine by high-performance liquid chromatography. *J. Chromatogr. B. Biomed. Sci. App.* **423**, 105–113 (1987).

81. H. A. Hussain, A. P. Roberts, P. Mullany, Generation of an erythromycin-sensitive derivative of Clostridium difficile strain 630 (630Deltaerm) and demonstration that the conjugative transposon Tn916DeltaE enters the genome of this strain at multiple sites. *J. Med. Microbiol.* **54**, 137–141 (2005).

82. Y. Zhao, S. B. Melville, Identification and characterization of sporulation-dependent promoters upstream of the enterotoxin gene (cpe) of Clostridium perfringens. *J. Bacteriol.* **180**, 136–142 (1998).

83. F. R. Blattner, G. Plunkett, C. A. Bloch, N. T. Perna, V. Burland, M. Riley, J. Collado-Vides, J. D. Glasner, C. K. Rode, G. F. Mayhew, J. Gregor, N. W. Davis, H. A. Kirkpatrick, M. A. Goeden, D. J. Rose, B. Mau, Y. Shao, The complete genome sequence of Escherichia coli K-12. *Science* **277**, 1453–1462 (1997).

84. E. P. Cato, J. L. Johnson, Reinstatement of Species Rank for Bacteroides fragilis, B. ovatus, B. distasonis, B. thetaiotaomicron, and B. vulgatus: Designation of Neotype Strains for Bacteroides fragilis (Veillon and Zuber) Castellani and Chalmers and Bacteroides thetaiotaomicron (Distaso) Castellani and Chalmers. *Int. J. Syst. Bacteriol.* **26**, 230–237 (1976).

85. H. Laroui, S. A. Ingersoll, H. C. Liu, M. T. Baker, S. Ayyadurai, M. A. Charania, F. Laroui, Y. Yan, S. V. Sitaraman, D. Merlin, Dextran sodium sulfate (DSS) induces colitis in mice by forming nano-lipocomplexes with medium-chain-length fatty acids in the colon. *PloS One* **7**, e32084 (2012).

Acknowledgments

We thank M. Garcia, V. Dangles-Marie, the mouse facility technicians, and the flow cytometry core at Institut Curie. We thank F. El Marjou and C. Jouhanneau for the generation of the LSL-MR1 transgenic mouse and S. Robine for the Villin-CreER mouse. We thank the ICGex NGS platform of the Institut Curie for technical help with single-cell RNA-seq and metagenomic experiments. ICGex is supported by the grants ANR10EQPX03 (Equipex) and ANR10INBS0908 (France Génomique Consortium) from the Agence Nationale de la Recherche ('Investissements d'Avenir' program), by the ITMO-Cancer Aviesann (Plan Cancer III) and by the SiRIC-Curie program (INCa-DGOS-465 and INCa-DGOS-Inserm_12554). We are grateful to the INRAE MIGALE bioinformatics facility for providing help, computing and storage resources. We thank D. Halpern (INRAE, Jouy-en-Josas, France) for his expertise and technical help with *B. thetaiotaomicron*. We thank J.J. Moon (Massachusetts General Hospital) for providing the LSL-MR1 backbone. We thank N. Manel and B. Chassaing for discussions and critical reading of the manuscript. We thank the NIH tetramer core facility (Emory University) for providing CD1d and MR1 tetramers. The MR1:5-OP-RU tetramer technology was developed jointly by J. McCluskey, J. Rossjohn, and D. Fairlie, and the material was produced by the NIH Tetramer Core Facility as permitted to be distributed by the University of Melbourne. The sequencing data generated in this study are available on the EBI ENA through the accession number PRJEB58263.

Funding

Supported by :

Institut National de la Santé et de la Recherche Médicale (OL, FL)

Institut Curie (OL)

Agence Nationale de la Recherche Grant JCJC ANR-19-CE15-0002-01 MAIT (FL)

Agence Nationale de la Recherche Grants MAIT (ANR-16-CE15-0020-01), diabMAIT (ANR-17-CE14-0002-02), MAITrepair (ANR-20-CE15-0028-01), ANR-10-IDEX-0001-02 PSL (OL) and MicrobMAIT (ANR-23-CE15-0036-01) (FL)

European Research Council (ERC-2019-AdG-885435) (OL)

Chaire de recherche from Rennes Métropole - 22C0451 (FL)

Fondation pour la Recherche Médicale - FDT202304016434 (MF)

Author contributions

Conceptualization: YEM, OL, FL; Methodology: MMa; Investigation: YEM, MF, AV, KF, CM, TD, HB, MS, BJ, VP, AB, SM, LC, AH, CP, EP, SR, FL; Formal analysis: MMe, HB; Funding

acquisition: OL, RR, FL; Supervision: OL, FL; Writing – original draft: FL; Writing – review & editing: All authors.

Competing interests

The authors declare no competing interests.

Data and materials availability

16S rRNA amplicon sequencing data, metatranscriptomic, metagenomic and single-cell RNAseq data are available on the EBI ENA under the accession number PRJEB58263. All the other data are available in the main text or the supplementary materials.

Figure legends

Figure 1: Bacterial production of MAIT ligands in the colonic mucosa. **A**. Left: To quantify MAIT ligands in intestinal contents, WT3-MR1 cells loaded with filtered intestinal contents are co-cultured with TCR-Tg T cells recognizing MR1:5-OP-RU complexes. Right: Activation of MR1:5-OP-RU-specific TCR-Tg T cells after co-culture with WT3 or WT3-MR1 cells pulsed with colon contents at indicated dilutions (n=3 mice per group. Data pooled from *N*=2). *p<0.05, **p<0.01 and ***p<0.001 by unpaired multiple *t* tests with FDR=1%. UD: undiluted. **B**. Left: MR1:5-OP-RU-specific TCR-Tg T cell activation after co-culture with WT3-MR1 cells pulsed with filtered luminal contents from control or antibiotic-treated mice. Right: MAIT ligand concentrations expressed as 5-OP-RU equivalent (n = 3-5 mice per group; representative of *N*=2). The dotted line indicates TCR-Tg T cell activation in absence of intestinal contents. *p<0.05 by unpaired multiple Mann-Whitney *U* tests with FDR=1%. **C**. Estimation of cecal bacterial numbers by qPCR amplification of 16S rRNA genes (data pooled from *N*=2). *p<0.05 by paired Wilcoxon test. **D**. Top: MR1:5-OP-RU-specific TCR-Tg T cell activation after co-culture with WT3-MR1 cells pulsed with lumen or mucosal cecal contents. Bottom left: Relative expression of CD25 and CD69 by MR1:5-OP-RU-specific TCR-Tg T cells in the indicated conditions (means ± SEMs, n = 9-10 mice; data pooled from *N*=2). **p<0.01 by paired multiple *t* tests with FDR=1%. Bottom right: MAIT ligand concentrations expressed as 5-OP-RU equivalent. ** p<0.01 by paired Wilcoxon test. **E**. Abundance of the indicated phyla in cecum. Columns indicate individual mice. **F**. Differentially

expressed metabolic pathways between lumen and mucosal bacterial communities (padj<0.001 by Mann-Whitney *U* test, LFC>0.5). **G**. Top: Riboflavin biosynthetic pathway gene expression in cecal lumen and mucosa (padj≤0.05 by Mann-Whitney *U* test). Bottom: Scheme of the riboflavin biosynthesis pathway. **H**. Taxonomy of total (left) and *ribD* (right) bacterial transcripts in lumen and mucosa. **I.** Species-level taxonomy of *ribD* transcripts in lumen and mucosa.

Figure 2: Dysanaerobiosis drives microbiota production of MAIT ligands. A. Cecal butyrate concentrations in control and streptomycin-treated mice. n=8 mice per group, *N*=1. ****p<0.0001 by unpaired Student's *t* test. **B**. PMDZ adduct and DAPI staining in the colon. TB: Tributyrin. The bar represents 50 μm. Quantification of PMDZ adduct staining at colon epithelial surfaces (each dot summarizes data from one mouse). Representative of *N*=2. **p<0.01 by unpaired Student's *t* test. **C**. MR1:5-OP-RU-specific TCR-Tg T cell activation after co-culture with WT3-MR1 cells pulsed with cecal contents from the indicated mice (n = 14 mice per group; data pooled from *N*=3). ***p<0.001, **p<0.01 by unpaired multiple *t* tests with FDR=1%. **D**. MAIT ligand concentrations expressed as 5-OP-RU equivalent (n=14 mice per group, data pooled from *N*=3). **p<0.01 and ****p<0.0001 by unpaired Mann-Whitney *U* tests. **E**. qPCR-based estimation of cecal bacterial numbers in the indicated mice. n=8 mice per group, *N*=1. **p<0.01 by unpaired Mann-Whitney *U* test.

Figure 3: Intestinal inflammation triggers riboflavin and MAIT ligand production by the microbiota. A. Cecal butyrate concentrations in control and DSS-treated mice. n=8 mice, *N*=1. ***p<0.001 by unpaired Student's *t* test. **B**. PMDZ adduct and DAPI staining in the colon. Quantification of PMDZ adduct staining at colon epithelial surfaces (each dot summarizes data from one mouse). Each dot summarizes data from 1 mouse. *N*=2. **p<0.01 by unpaired Student's *t* test. **C**. Left: MR1:5-OP-RU-specific TCR-Tg T cell activation after co-culture with WT3-MR1 cells pulsed with cecal contents from the indicated mice (mean ± SEMs, n= 3 mice per group,

representative of *N*=2). *p<0.05 by unpaired multiple *t* tests with FDR=1%. Right: MAIT ligand concentrations expressed as 5-OP-RU equivalent (n=6 mice per group, data pooled from *N*=2). **p<0.01 by unpaired Mann-Whitney *U* test. **D**. Percentage of mouse transcripts in cecum from the indicated mice. *p<0.05 by unpaired Mann-Whitney *U* test. **E**. Predicted cell-type enrichment in cecum of DSS-treated as compared to control mice (Methods). **F**. Differentially expressed mouse genes in cecum lumen upon DSS treatment. **G**. Bacterial metabolic pathways differentially expressed between control and DSS-treated mice (padj<0.01 by Mann-Whitney *U* test, LFC>0.5). **H**. Differentially expressed riboflavin biosynthetic pathway transcripts between control and DSS-treated mice (padj<0.01 by Mann-Whitney *U* test). **I**. Cecal riboflavin concentration (n=7-8 mice per group, representative of *N*=2). The dotted line indicates homeostatic plasma riboflavin concentration. ***p<0.001 by unpaired Student's *t* test. **J**. Principal component analysis of cecal DNA reads at the family level in control and DSS-treated mice. **K**. Phylum-level taxonomy of total bacterial DNA (left) or RNA (right) reads from the cecum. **L**. Phylum-level taxonomy of *ribD* DNA (left) or RNA (right) reads from the cecum. **M**. Species-level taxonomy of *ribD* transcripts.

Figure 4: MAIT ligands cross the intestinal barrier and are presented to MAIT cells in various tissues. A. Assay used to assess intestinal permeability to ligands (also Methods). **B**. TCR-Tg T cell activation in the indicated conditions (data pooled from *N*=2). **p<0.01 by paired multiple *t* tests with FDR=1%. **C**. Identification of MAIT cells from the colon of B6-MAIT^{Cast} mice. Pooled data from *N*=3. **D**. *Nr4a1*-GFP expression by MAIT (top) and iNKT (bottom) cells. Data pooled from *N*=3. ns p>0.05, *p<0.05, **p<0.01 and ***p<0.001 by unpaired multiple Mann-Whitney tests with FDR=1%.

Figure 5: MAIT cells reduce colitis severity. A. *Nr4a1*-GFP expression by MAIT cells from the indicated mice. Both LSL-MR1^{+} and LSL-MR1^{-} mice carried the Villin-CreER Tg and received

tamoxifen. Pooled data from *N*=3. ****p<0.0001 by unpaired Mann-Whitney *U* test. **B**. Areg expression by colonic MAIT cells from the indicated mice. n= 7 mice per group. Data pooled from *N*=2. ***p<0.001 by unpaired Student's *t* test. **C**. Cytokine production by colonic MAIT cells from control mice and from mice with chronic colitis. n=9-11 mice per group. Data pooled from *N*=2. **p<0.01, ***p<0.001 and ****p<0.0001 by unpaired Student's *t* tests. **D**. Mouse body weight following mock or chronic DSS treatment. n=12-13 mice per group. Data pooled from *N*=3. **p<0.01 and ***p<0.001 between DSS-treated $Mr1^{+/+}$ and $Mr1^{-/-}$ mice, by unpaired multiple *t* tests with FDR=1%. **E**. Top: Hematoxylin and eosin staining of colon from the indicated condition. Representative 2X and 10X magnifications are shown. Bottom: Investigator-blinded pathology assessments in the indicated conditions. n=5-7 mice per group. Data representative of *N*=3. ns p≥ 0.05, *p<0.05, **p<0.01, ***p<0.001 and ****p<0.0001 by unpaired Student's *t* tests. **F-G.** Principal component analyses of bacterial Families in $Mr1^{+/-}$ and $Mr1^{-/-}$ B6-$MAIT^{Cast}$ mice either untreated (**F**) or upon chronic DSS-induced colitis (**G**). Symbols indicate the cage of origin.

Figure 6: MAIT cells protect against inflammation-induced colorectal cancer. **A.** Left: Representative images of rectum after inflammation-induced CRC. Right: rectal tumor numbers in the indicated mice. Pooled data from *N*=2. **p<0.01 by unpaired Student's *t* test. **B.** UMAP of colonic MAIT cells isolated from control (AOM) or colitic (DSS) mice analyzed by single-cell RNAseq. The relative contribution of MAIT cells from control and colitic mice to each cluster is indicated. **C.** Expression of selected genes by MAIT cells from the indicated UMAP clusters. **D.** *Il22* expression by single-cell RNAseq in colonic MAIT cells. **E**. Tissue-repair gene signature expression in the indicated clusters. The dashed bar represents the median score. *p<0.05, ***p<0.001 and ****p<0.0001 by unpaired Student's *t* tests. **F**. Schematic summary of the main findings of the study.

Supplementary Materials

Materials and Methods

Study design

Prior to inclusion in experimental groups, mice from different litters were co-housed, or cage contents were mixed for at least two weeks in order to normalize microbiota. Individual mice were randomly assigned to experimental groups. The assessment of colitis and colorectal cancer severity was performed by scientists blinded to mouse genotypes (*Mr1*$^{+}$ or *Mr1*$^{-/-}$), which remained concealed until pathology measurements were completed. The number of independent experiments performed, *N*, is indicated in figure legends.

Mice

C57BL/6J (B6) and B6-CD45.1 mice were purchased from Charles River Laboratories. iVα19 and iVα19 Vβ8 TCR transgenic Cα$^{-/-}$ B6 mice, WT and *Mr1*$^{-/-}$ B6-MAIT^{Cast} mice have been described(*19*, *64*). *Nr4a1*-eGFP mice(*36*) were imported from the MMRRC (UC Davis). OTII mice(*65*) were maintained on a RAG$^{-/-}$ background. All mice were bred and maintained on a standard chow diet in SPF conditions at Institut Curie. All experiments were performed according to national and international guidelines and were approved by the Institut Curie Ethic committee (APAFIS#25203-2020042318109119, #24245-2020021921558370, #IOI68-2017060909448377 and #26939-2020082515024782 v1). To generate the Lox-stop-Lox-MR1 (LSL-MR1) transgenic mouse, a DNA segment containing a stop cassette flanked with loxP sites upstream of the murine *Mr1* gene was prepared by digestion of the pOD2G-LS CAGGS (7279 bp) plasmid(*66*) (a gift from J. J. Moon, Massachusetts General Hospital) with the enzymes HindIII and SpeI allowing the insertion of a full length MR1 cDNA. Efficient induction of MR1 protein expression under the control of the chicken actin promoter was validated in HEK293 cells co-transfected with a Cre expression vector. The construct was then injected into pronuclei of fertilized C57BL6/N oocytes. Founders were crossed to transgenic mice bearing either a CD11c-Cre transgene(*67*) or a tamoxifen-dependent Cre recombinase expressed under the control of the Villin promoter(*38*).

Antibiotic treatments, colitis induction, and tamoxifen administration

Female mice aged 6-10 weeks at the start of the experiments were used. For microbiota depletion, B6/J mice were given four antibiotics (vancomycin (0.5 g/l, Mylan), ampicillin (10 g/l, Coophavet), metronidazole (1 g/l, B Braun) and neomycin (1g/l, Coophavet) in the drinking water supplemented with 2% sucrose for 7 days. Fresh antibiotic solutions were provided after 3 days of treatment. Streptomycin (2.5 mg/ml, Sigma, S9137) was provided for 4 days in the drinking water supplemented with 2% sucrose. When indicated, streptomycin-treated mice also received tributyrin (5 g/kg) (Sigma, T8626) by oral gavage each day for 4 days. For fungal depletion, fluconazole (0.5 mg/ml, Sigma-Aldrich) was provided in the drinking water for 7 days.

Acute colitis was induced in B6/J mice by adding 2% (wt/vol) DSS (molecular weight: 36,000–50,000 Da; MP Biomedicals) to the drinking water for 7 days or until mice had lost 15% of initial weight. For modelling chronic colitis, B6-MAIT^{Cast} mice received successive 5-day DSS treatments, each with increasing DSS concentrations, followed by 4 days with water only. Co-housed *Mr1*$^{+/+}$ and *Mr1*$^{-/-}$ mice received 3 cycles of DSS prior to clinical pathology assessment. Pathology assessment was performed by an investigator blind to mouse genotypes. *Mr1*$^{+/+}$ mice received 4-5 cycles until mice had lost weight for 2 consecutive weeks prior to phenotypic

analyses of MAIT cells. Control groups (Mock) received only water. For inducible MR1 over-expression, all mice were injected intraperitoneally with 2 mg tamoxifen (T5648, Sigma-Aldrich) in a corn oil-ethanol mixture once per day for 3 consecutive days. Tissues were collected 24 h after the last injection.

Colorectal cancer models

The AOM/DSS model(*68*) was used as a model of colitis-induced colorectal cancer. Male and female *Mr1*$^{+}$ and *Mr1*$^{-/-}$ B6-MAIT^{Cast} mice aged at least 12 weeks were co-housed for at least 2 weeks before the start of the experiment to normalize the microbiota. The mice received a single intraperitoneal injection of saline or of azoxymethane in saline (10mg/kg) (Sigma Aldrich A5486-25MG). Mice were then treated 3 times with DSS (2.5%) in the drinking water for 4 days, followed by 17 days on water. The first DSS treatment started 4 days after AOM injection and mice were euthanized 110-130 days later. Colonic and rectal tumors were counted by an investigator blind to mouse genotypes. For orthotopic colorectal cancer development, co-housed female B6-MAIT^{Cast} *Mr1*$^{+}$ or *Mr1*$^{-/-}$ mice aged 12-18 weeks were anesthetized and implanted intrarectally with 2 x 10^6 MC38 cells. Colorectal tumors were counted 11 days later by an investigator blind to mouse genotypes.

Cell isolation

Spleens were mashed over 40 µm cell strainer to create single cell suspensions followed by red blood cell lysis. Livers were mashed over 100 µm cell strainer and centrifuged over Histopaque 1077 (Sigma) layers to isolate the lymphocyte-containing fraction. Colons were opened longitudinally and cut into approximately 0.5 cm pieces. Dissociation of epithelial cells was performed by incubation with constant stirring in HBSS w/o Ca/Mg (Life Technologies) containing 5 mM EDTA (5mM; Thermo Fisher Scientific), DTT (1 mM; Euromedex), and 5% FCS twice for 20 min at 37 °C. After each step, samples were vortexed and the epithelial fraction discarded. Tissue fragments were then washed in HBSS and enzymatic digestion was performed in CO_2-independent medium (Life Technologies) containing collagenase D (1 mg/ml; Roche), liberase TM (0.17 U/ml; Roche) and DNase I (100 µg/ml; Roche) on a shaker for 30 min at 37 °C. Colon fragments were then dissociated with a gentleMACS dissociator according to the manufacturer's instructions (Miltenyi). Lymphocytes were collected at the interface of a 40%/80% Percoll gradient (GE Healthcare).

Tetramers and flow cytometry

CD1d tetramers loaded with PBS-57 and conjugated to BV421, and MR1 tetramers loaded with 5-OP-RU and conjugated to PE were provided by the National Institutes of Health (NIH) tetramer core facility (Emory University). Cell suspensions prepared from various tissues were stained in PBS, 2% FCS, 2 mM EDTA complemented with rat anti-mouse CD16/CD32 antibody (clone 2.4G2 produced in-house) to block non-specific binding to Fcγ receptor. Tetramer staining was performed at room temperature for 30 min. Surface staining was performed at 4 °C with fluorescently labelled antibodies and fixable viability dye eFluor780 (eBioscience, Hatfield, UK). MR1:5-OP-RU-specific TCR-Tg T cells were identified as shown in Fig. S1A. MAIT and iNKT cells were identified as shown in Fig. S5C. A list of the antibodies and reagents used in the study is provided in Table S6.

Fixation and permeabilization were performed for intranuclear staining (FoxP3 staining kit; eBioscience) and intra-cytoplasmic staining (Cytofix/Cytoperm kit; BD Biosciences) according to the manufacturer's instructions. For intra-cytoplasmic staining, cells were cultured for 3 h at 37 °C in complete RPMI in the presence of GolgiPlug (1:1000; BD). Cultured cells were subsequently stained for surface antigens as above. Cells were fixed and permeabilized, washed, and incubated for 30 min at 4 °C with anti-IL17 (TC11-18H), -IL22 (IL22JOP) and -IFNγ (XMG1.2). Cells were then stained overnight with anti-amphiregulin-biotin (BAF989) followed by FITC- or BV605-conjugated streptavidin. In some experiments, non-fixed dead cells were stained with the DAPI staining solution and directly analyzed by flow cytometry. Cells were acquired either on Cytoflex (Beckman), LSRII (BD Biosciences) or Fortessa (Becton Dickinson), and the results were analyzed with FlowJo V10.2 (Treestar).

Single-cell RNA sequencing

Mice injected with AOM or treated with DSS (9 mice per group) were sacrificed 53 days after AOM injection or 3 days after the end of the third DSS treatment. Colon MAIT cells were identified as live $CD11c^-B220^-CD19^-TCRb^+CD44^+$MR1:5-OP-RU tetramer+ and FACS-sorted into PBS containing 0.04% sterile bovine serum albumin (Sigma) using the BD FACSAriaIII. Sorted MAIT cells were counted and processed for 3' v3 single-cell RNAseq according to manufacturer's instructions (10X Genomics). Reads were aligned to the mm10 genome using CellRanger (6.0.0) and analyzed by Seurat (4.1.0) package in R (4.1.0). Contaminating cells (B lymphocytes, macrophages, epithelial cells) and cells with high mitochondrial content were filtered out. Data were normalized using default parameters. The 2,000 (AOM) and 3,000 (DSS) most variable features were selected. Both datasets were integrated using default parameters without the SC transform option. Reduction of dimensions was performed using 30 principal components and a resolution of 0.8. Differential expression (DE) analysis was performed on assay RNA using the classical DE function FindAllMarkers(), but using logistic regression and taking into account batch effect in the logistic regression model. To compute a tissue-repair score, we aggregated the expression of the following genes (Linehan et al, 2018, Table S4): *Hbegf, Csf2, Mmp25, Cxcl10, Areg, Jag1, Tnf, Pdgfb, Tgfb3, Cxcl2, Furin, Il1b, Tgfb1, Hif1a, Thbs1, Vegfb, Hmgb1, Ptges2, Disp1*.

5-OP-RU preparation

5-A-RU was synthesized as described(*6*, *69*). For preparation of 5-OP-RU, 5-A-RU was incubated with a 4-fold excess of methylglyoxal (Sigma) for 10 min at room temperature.

***In vitro* validation of the *Nr4a1*-eGFP mouse**

Splenic T cells from a transgenic *Nr4a1*-eGFP mouse were isolated by negative cell enrichment using the Magnisort mouse T cell enrichment kit (Thermo Fisher Scientific). Isolated cells were cultured at a density of 20 x 10^6 /ml in complete RPMI and stimulated with either recombinant mouse IL-12 (10 ng/ml) and IL-18 (12.5 ng/ml) or with 10 nM 5-OP-RU in the presence of the murine embryonic fibroblast cell line WT3 engineered to overexpress MR1(*20*) (WT3-MR1 cells, 5 x 10^6/ml) for 16h at 37 °C. GolgiPlug was added during the final 6h of culture. MAIT cells were then analysed for *Nr4a1*-GFP expression and IFNγ production.

***In vitro* detection of MAIT ligands**

To detect intestinal MAIT ligands, 100 mg of luminal contents were collected from the cecum or colon. Feces were collected from cage floors immediately after defecation. Samples were weighted and dissolved in complete RPMI medium (RMPI without folic acid supplemented with 10% FCS, penicillin and streptomycin), and kept on ice. Tubes were vortexed to homogenize the mixture and centrifuged at maximum speed for 1 min at 4 °C. Supernatants were filtered through a 0.22-µm-pore-size filter and loaded at different dilutions on 10^5 WT3-MR1 cells for 2 h 30 min at 37 °C. WT3-MR1 cells, a mouse embryonic fibroblast cell line engineered to overexpress MR1, has been described elsewhere(*41*). WT3-MR1 cells were then washed and co-cultured overnight at a 1:1 ratio with total splenocytes from a Vα19 TCR Tg $Cα^{-/-}$ or Vα19Vβ8 TCR Tg $Cα^{-/-}$ mouse. TCR Tg splenocytes were also incubated with unloaded WT3-MR1 cells to measure background activation. Cells were then harvested and stained for CD25 and CD69 expression on 5-OP-RU:MR1-specific T cells. The resulting activation was internally normalized to the unloaded condition (unloaded WT-MR1 cells). In each experiment, MAIT ligand concentrations were estimated using a standard curve prepared with serial dilutions of synthetic 5-OP-RU. For comparing lumen and mucosal samples, 50 mg of luminal contents and 50 mg of mucosal scrapings were sampled by scraping biomass from intestinal walls with a sterile scalpel. Samples were then processed as described for luminal contents. For comparing 2-weeks-old and 3-months-old samples, 15 mg of colon contents were harvested from both groups and processed as described above for luminal contents.

Intestinal permeability to 5-OP-RU

75 µl of PBS containing 12 nmoles of OVA 323-339 peptide (Invivogen) mixed with the indicated amount of 5-OP-RU (0.1 – 100 pmoles) were introduced into the lumen of freshly isolated colons from healthy mice, using a p200 pipette. Colon segments were then immersed in complete RPMI medium at 37 °C in a well on top of mixed MutuDC(*85*) and WT3-MR1 cells, for OVA and 5-OP-RU presentation, respectively. As positive control, ligand solutions were also added directly on top of mixed antigen presenting cells. Colon segments were removed from the wells after 10 min of incubation. For the measurement of antigen-presentation, splenocytes from a Vα19 TCR Tg $Cα^{-/-}$ mouse and from a OTII-$Rag2^{-/-}$ mouse were cultured overnight with antigen presenting cells at respectively 1:1 and 1:10 ratios. 5-OP-RU-specific and Ova-specific splenocytes were identified as MR1:5-OP-RU tetramer+ and Vα2+ T cells, respectively, and analysed for surface expression of CD25 and CD69.

Intestinal sample collection for nucleic acids extraction

Immediately after euthanasia, luminal contents and mucosal scrapings were collected from the cecum. Cecal contents were resuspended in RLT lysis buffer (Qiagen) supplemented with acid-washed glass beads (Sigma). Bacteria were lysed using a Fast Prep bead beater (MP Biomedicals) (3 times 1 min at 6.5 m/s). Total DNA and RNA were purified using the AllPrep DNA/RNA Kit (Qiagen). On-column DNA digestion was performed prior to RNA elution.

16S rRNA gene PCR amplification and sequencing

16S rRNA gene sequencing was performed in-house or at the University of Minnesota Genomics centre with similar results. In-house library preparation was performed as described(*86*). Briefly, a single PCR step was used for amplification of the V3-V4 region of the 16S rRNA gene and for dual-index labelling of each sample. PCR amplification was performed using the Accuprime Pfx

DNA polymerase (ThermoFisher). PCR products were purified (AMPure XP beads, Beckman Coulter) and sequenced on MiSeq (Illumina, USA) to generate paired-end 300-bp reads.
To study the effect of *Mr1* on the microbiota at steady-state, the V3-V4 region was amplified (using the Accuprime Pfx DNA polymerase) from DNA isolated from the feces of co-housed *Mr1*$^{+/-}$ and *Mr1*$^{-/-}$ B6-MAIT^{Cast} mice. PCR products were purified on agarose gel (1.5%) using the Qiaquick gel extraction kit (Qiagen). After gel extraction, sequencing was performed on MiSeq (Illumina, USA) to generate paired-end 300-bp reads.

Bioinformatic analysis of 16S rRNA sequencing data

Adapter sequences were trimmed from the raw fastq files using Cutadapt v 2.10(*87*). Reads were further corrected for known sequencing error using SPAdes (v3.14.1 – PMID: 32559359) and then merged using PEAR (v0.9.11 – 24142950). ASVs were identified using a Vsearch pipeline (v2.21.1 – 27781170) designed to dereplicate (--derep_prefix –minuquesize 2) and cluster (--unoise3) the merged reads, as well as check for chimeras (uchime3_denovo). Taxonomic classification of ASVs was performed using the classifier from the RDPTools suite (v2.13 – 24288368). Representative ASVs sequences were taxonomically assigned using the RDP classifier with a SAB score ≥0.5. Downstream analyses and visualization were performed in the R environment v 4.0.4 (R Core Team 2019). Metabolic pathway abundance in each sample was predicted using PICRUSt2(*88*) and differentially abundant pathways were identified using LEfSe(*89*).

Metatranscriptomic and metagenomic data generation

For metatranscriptomic analyses, total RNA was prepared from the cecum mucosa and lumen of 6 non-treated mice, and from the cecum lumen of 8 untreated mice and 8 mice treated with 2.5% DSS for 7 days followed by 2 days on water. DNA was also isolated from the cecum lumen of the same mock- and DSS-treated mice for paired metagenomic analyses (see below for metagenomic library preparation). Sequencing libraries were prepared from DNase-treated total RNA using the Illumina Stranded Total RNA Prep Ligation with Ribo-Zero Plus kit. Indexed libraries were sequenced (SR100) on a NovaSeq (Illumina). 23-80 M reads (mean 54.4 M +/-15.3 M) were obtained for each library.
For metagenomic analyses, sequencing libraries were prepared from cecum lumen DNA using the KAPA HyperPrep Library PCR-Free kit (Roche). Indexed libraries were sequenced (SR100) on a NovaSeq (Illumina). 5.4-71 M reads (mean 42 M +/-22 M) were obtained for each library.

Metatranscriptomic and metagenomic data analysis

Single end reads were quality checked and trimmed using TrimGalore v0.6.6 (https://github.com/FelixKrueger/TrimGalore). Host reads were identified by aligning metatranscriptomes and metagenomes against the mouse genome (http://ftp.ensembl.org/pub/release-102/fasta/mus_musculus/dna/Mus_musculus.GRCm38.dna.primary_assembly.fa.gz) using STAR v2.7.7(*90*). Ribosomal reads were removed from metatranscriptomic datasets using sortmerna v4.2.0(*91*). Finally, remaining non-host non-ribosomal reads were mapped against the iMGMC mouse gene catalogue(*92*) using bwa v0.7.17-r1188 with default parameters. Read counts aligned to the iMGMC gene catalogue were obtained from bam files processed with featureCounts v2.0.1(*93*). Only genes with at least 50 total reads were selected for downstream analyses. For analysis of microbial gene expression,

reads were binned by KEGG categories at the level of metabolic pathways or at the level of genes. The binned features (either pathways or genes) were then used as input in DESeq2(*39*) to identify differentially abundant features, which were displayed on heatmaps using the pheatmap R package v 1.0.12. The same analysis pipeline was applied to the published metatranscriptomic dataset(*94*) stored under the accession number E-MTAB-4082 and downloaded from EBI ENA. To predict which mouse cells are present in cecum during DSS treatment, the top 200 mouse transcripts with increased abundance in cecum of DSS-treated mice were used as input in the Immgen Microarray v1.

Estimation of bacterial number in intestinal samples

Total bacterial numbers from intestinal samples were estimated by TaqMan qPCR quantification of bacterial 16S rRNA (LightCycler 480 Instrument II, Roche). The universal 16S rRNA gene primers and probe sequences used in this study are as follow(*95*): 16S Forward: 5'TGGAGCATGTGGTTTAATTCGA3'. 16S Reverse: 5'TGCGGGACTTAACCCAACA3'. Probe: 5'CACGAGCTGACGACA(AG)CCATGCA3'. A standard curve was built using *Escherichia coli* MG1655 DNA to convert the threshold cycle (Ct) values into colony-forming unit (CFU) equivalents.

Short-chain fatty acid (SCFA) analysis

SCFA analysis was carried out as described previously(*96*), with slight modifications. Samples were water-extracted and proteins were precipitated with phosphotungstic acid. A volume of 0.3 µl of the supernatant fraction was injected into a gas–liquid chromatograph (Agilent 6890; Les Ulis, France) equipped with a split-splitless injector, a flame-ionization detector and a capillary polyethylene glycol column (15 m x 0.53 mm, 0.5µm). Carrier gas (H_2) flow rate was 10 ml/min and inlet, column and detector temperatures were 200°C, 100°C and 240°C, respectively. Between each sample injection, the column was cleaned by increasing the temperature from 100°C to 180°C (20°C/min) followed by holding at 180°C for 2 min before returning to 100°C for the next analysis. 2-Ethylbutyrate was used as an internal standard. Samples were analyzed in duplicate. Data were collected and peaks integrated with the OpenLab CDS Chemstation Edition software (Agilent, Les Ulis, France).

Riboflavin dosage

Cecum contents from 8 untreated mice and 7 mice treated with 2.5% DSS for 7 days were harvested, weighted and dissolved in water. After centrifugation (14,000 rpm, 5 min, 4 °c), supernatants were passed through a 0.22 µm filter and analysed by reverse-phase HPLC following a method adapted from Lopez-Anaya et al(*97*). Briefly, samples were diluted 1:20 in distilled water, then 1:2 in acetonitrile. Diluted samples were vortexed for 1 min followed by centrifugation (4,000 rpm, 10 min, 12°c). Supernatants were transferred into glass tubes and mixed with 2 mL chloroform followed by vortexing for 1 min. Samples were centrifugated (4,000 rpm, 10 min, 12 °c) and 20 mL of supernatant were injected on a Uptisphere C18 ODB-15QK 3m 4.6 x 150 mm column (Interchim) with isocratic elution mode at 1 mL/min. The mobile phase contained 700 mL of buffer (1.35g potassium phosphate, 1g ammonium acetate in 700 mL of water) and 300 mL acetonitrile (potassium phosphate 10 mM, ammonium acetate 12.3 mM). Riboflavin was detected by fluorescence after excitation at 445 nm and detection at 530 nm. Retention time of riboflavin was about 8 min.

Detection of intestinal hypoxia

Pimonidazole (PMDZ) (Sigma-Aldrich) was administered at 60 mg/kg by intraperitoneal injection 1 h prior to sacrifice. Colon samples were fixed in formalin solution 10 % neutral buffer (Sigma-Aldrich). Paraffin-embedded sections were blocked with protein block (Dako, X0909) and treated with avidin/biotin blocking reagents (Dako, X0590) followed by overnight incubation at 4 °C with either biotinylated or purified mouse monoclonal anti-PMDZ antibody (Hypoxyprobe^{TM}-1) at 1.2 µg/ml according to the manufacturer's instructions. Sections stained with purified anti-PMDZ primary antibody were then incubated for 30 min with *biotinylated* anti-mouse *IgG* secondary *antibody* (Vectastain). Negative control sections were treated identically except that primary antibody was substituted with control antibody (BD) for overnight incubation. All sections were then incubated for 30 min with Alexa546-conjugated Streptavidin (ThermoFisher). Tissues were counterstained with DAPI. PMDZ staining was quantified using Fiji and plotted as fluorescence intensity per 400 µm^2.

Individual bacterial cultures

All bacterial strains were first grown anaerobically (5% H_2, 5% CO_2, 90% N_2). *C. difficile* 630Δ*erm*(*98*)*, C. perfringens* SM101(*99*)*,* and *E. coli* MG1655(*100*) in Brain Heart Infusion (BHI, Difco) and *B. thetaiotaomicron* VPI-5482(*84*) (collection of S. Rabot, INRAE, Jouy en Josas, France) in M17 (Difco) supplemented with glucose 0.5 % and hemin 5 µM (Sigma-Aldrich). An overnight liquid preculture was diluted in 10 mL fresh medium 1/1000 for *E. coli* and *C. perfringens,* 1/50 for the other strains and grown anaerobically until late exponential growth phase. After respectively 3 h for *E. coli* and *C. perfringens,* 8 h for *B. thetaiotaomicron* and 6 h for *C. difficile*, cultures were distributed in 24-well plates, 1 mL per well and placed in aeroby at 37°C. Culture supernatants were harvested after 0 and 60 min air-exposure and fast frozen in liquid nitrogen. MAIT ligands were quantified in 0.22 µm-filtered supernatants using the MAIT ligand quantification bioassay.

Assessment of intestinal pathophysiology

In chronic DSS experiments, the spleen and colon were isolated from each mouse. Individual spleen tissues were weighed. The entire colon was fixed in formalin solution 10% neutral buffer, embedded in paraffin and stained with hematoxylin and eosin (H&E). H&E-stained sections of the colon were analysed for colitis severity in an investigator-blinded manner. Epithelial damage (architectural lesion), inflammatory cell infiltration and crypt length were scored using the histopathological scoring system described previously(*85*).

Statistical analyses

Statistical analyses and graphical representations related to the microbiome pipeline were conducted in R (v 4.0.4) (R Core Team 2019) with the R package ggplot2 v 3.2.0. All other statistical analyses were performed with Prism software (GraphPad). Two-tailed *P* values were determined using Wilcoxon's and Mann–Whitney's tests for paired and non-paired samples, as appropriate. A false discovery rate of 1% was calculated for multiple *t* tests and multiple Mann-Whitney's tests using the 2-stage step-up method of Benjamini, Krieger and Yekutieli.

El Morr et al, Figure 1

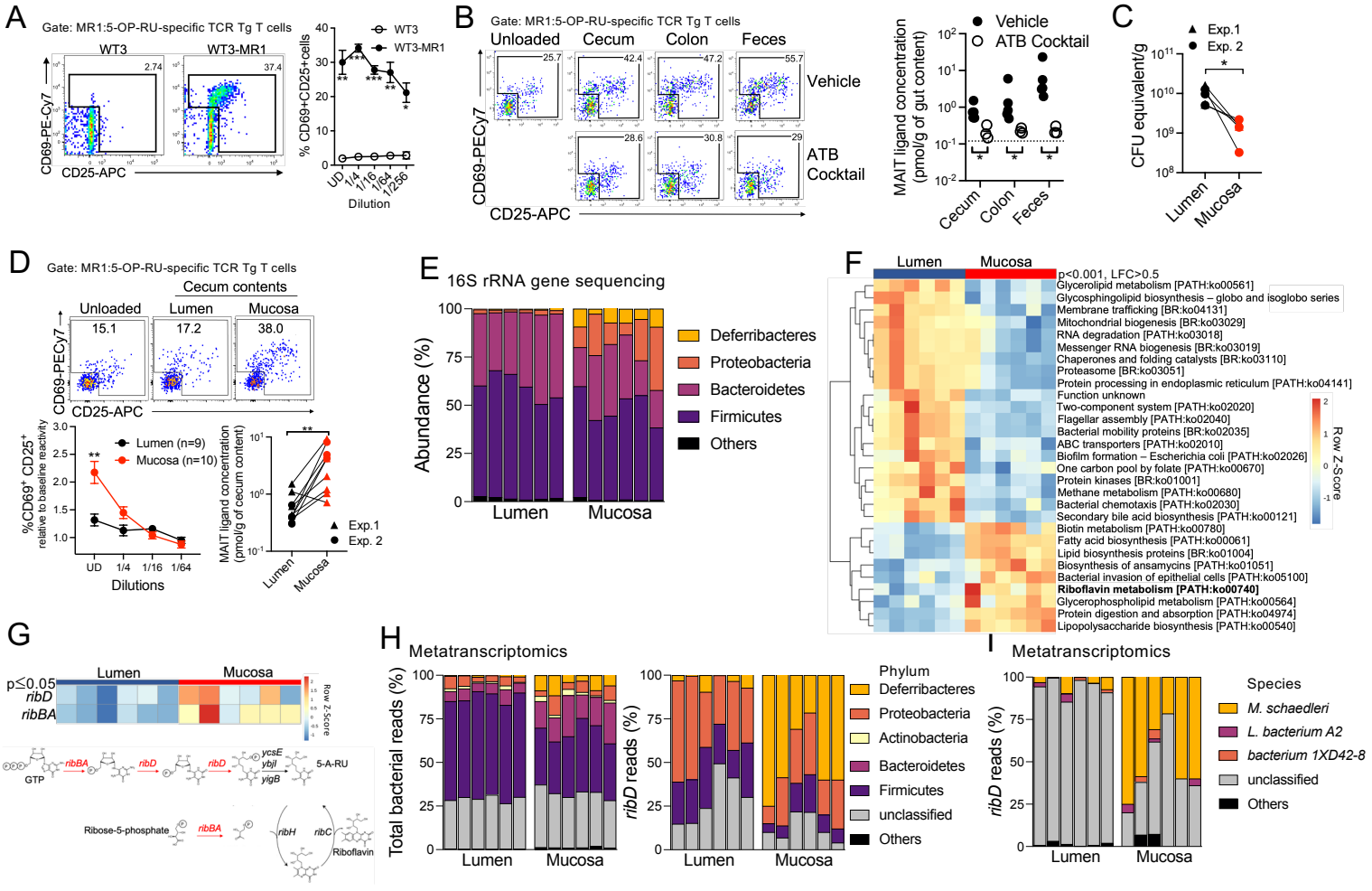

El Morr et al, Figure 2

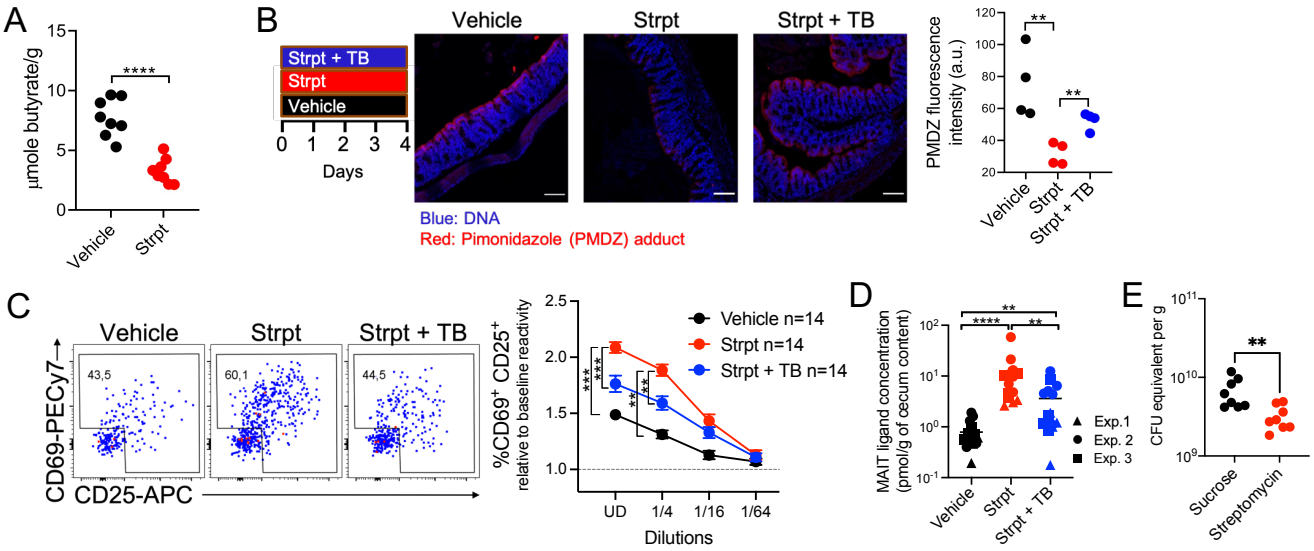

El Morr et al, Figure 3

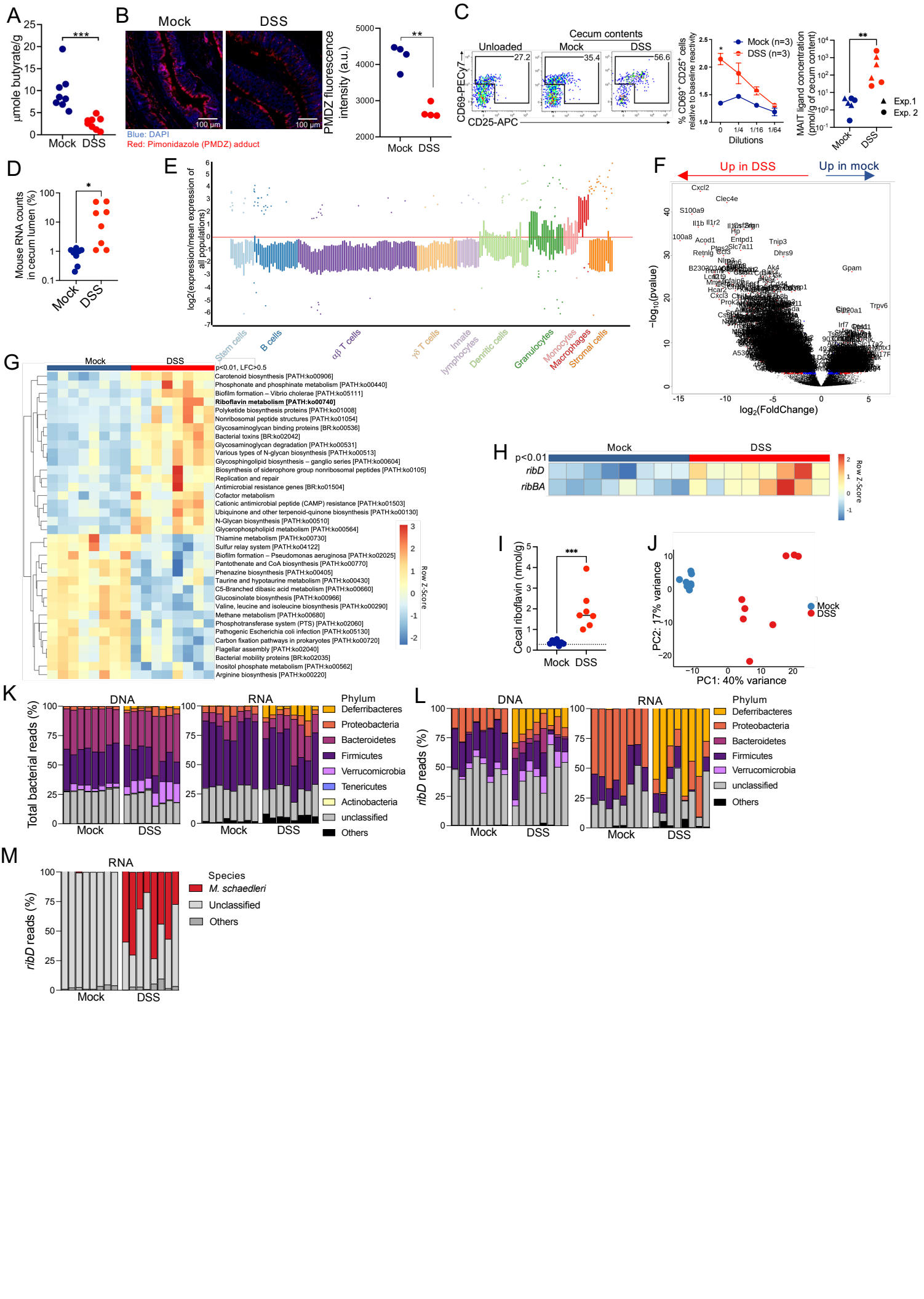

El Morr et al, Figure 4

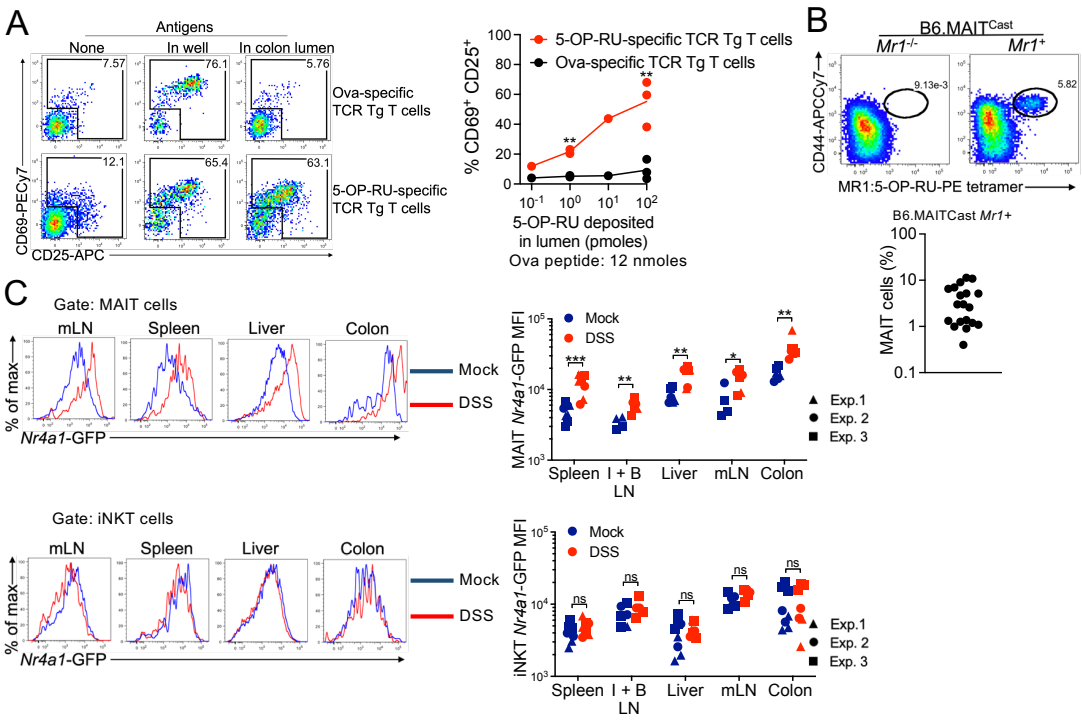

El Morr et al, Figure 5

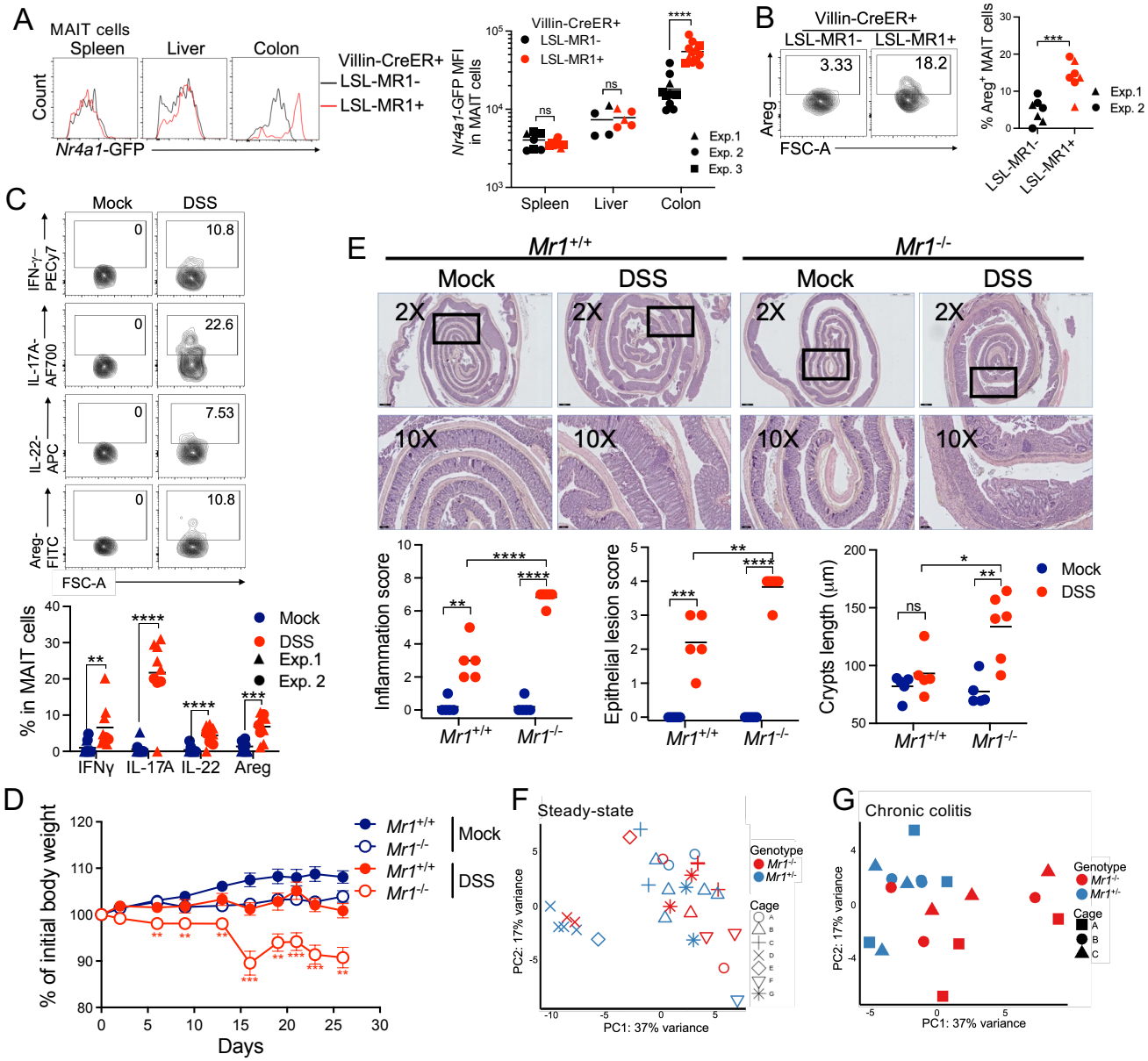

El Morr et al, Figure 6